Contents

Introduction

Quantum information processing is a new and rapidly developing area of quantum physics. The main difference to conventional computer science is the idea to use coherent superpositions of quantum states to store and process information in parallel.
Possible candidates for the hardware implementation of quantum information carriers are isolated atoms and photons. The recent experimental advances in quantum optics allow us to prepare not only pure quantum systems but also promise to realize controllable coherent manipulation of these systems.

Single ion trapping and manipulation techniques are among the most advanced implementations of quantum information processing hardware [Sac00], [Bla00]. Interaction between ions can be achieved via coupling to a common vibrational mode. However, the Coulomb interaction of the system with the environment, especially with stray electromagnetic fields, leads to decoherence and, therefore, to the loss of stored quantum information.

An alternative for storing and manipulating quantum information is the use of neutral atoms [Mon02]. They are not electrically charged and therefore interact with each other and the environment much more weakly. To induce controlled interaction between neutral atoms different schemes were proposed: controlled cold collisions [Jak99], induced dipole-dipole interaction [Bre99], magnetic spin-spin interaction [You00] and cavity quantum electrodynamics (CQED) [Pel95].

CQED is a promising scheme to realize controlled atom-atom interaction. In this scheme two neutral atoms are strongly coupled to a cavity and interact via exchange of a cavity photon. Therefore the cavity field is used as a quantum information bus between otherwise noninteracting neutral atoms.
The two main requirements for the realization of two-qubits gates based on single neutral atoms and cavity QED are the strong coupling between atom and cavity and the possibility to control the interaction strength and the interaction time. Since the atom-cavity interaction is strongly position dependent, it is necessary to control

the exact position of the atom inside the cavity.
A number of CQED experiments with neutral atoms have been carried out in the microwave regime, where the above requirements have been satisfied. In these experiments, Rydberg atoms interact with photons in a microwave cavity [Hag97], [Rau00], [Rai01].
In the current approaches to cavity QED experiments in the optical regime a beam of cold atoms is directed into the cavity [Gri95] or a cloud of atoms launched [Pin00], [Hor02] or dropped [Hoo00] into the cavity. These approaches allow to reach the regime of strong coupling between atoms and cavity, but intrinsically they do not allow to control the atomic external degrees of freedom, which is necessary to realize controlled interaction of two neutral atoms via a cavity photon.
Therefore, the present experimental challenge of optical CQED is to control the external degrees of freedom of atoms - time, position and number of neutral atoms interacting with the cavity mode.

Our strategy to realize this is to use the recently developed "optical conveyor belt" as a tool to move single atoms over distances up to 1 cm in a standing wave dipole trap [Fre00], [Kuh01], [Sch01]. It will allow us to controllably transport a desired number of cold Cs atoms from a Magneto optical trap (MOT) into the cavity mode (see Fig. 1).

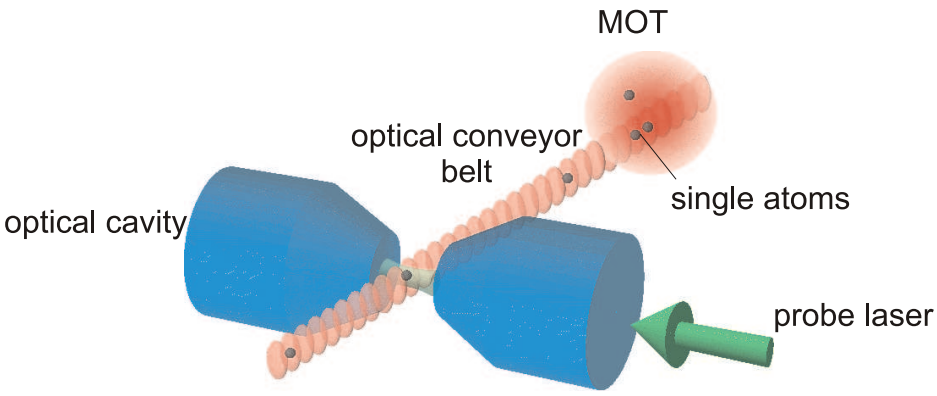

Figure 1: Single Cs atoms are cooled in a MOT, and an optical conveyor belt is used to deterministically transport them into a cavity

The task of this work is the construction and stabilization of such a high finesse cavity.
A sufficient coupling strength between the atoms and the cavity photon can only be achieved in an extremely small electromagnetic mode volume. This requires the mirror spacing of the cavity to be of the order of 100 μm. In addition to the challenge of mounting such a microcavity it is necessary to stabilize it on the atomic transition

using a lock laser which is far detuned to avoid its interaction with the atoms. For this purpose an additional low finesse cavity transfers the absolute stability from a laser stabilized to a Cs spectroscopy to this lock laser. Implementing this necessary chain of locks I succeeded to continuously lock a high finesse microcavity.

Chapter 1

Theoretical background

1.1 Introduction to optical resonators

An optical cavity (also known as optical resonator) is the central object of this work. The goal of this section is to derive the properties of optical resonators.

1.1.1 Transmission spectrum

In order to derive the properties of the cavity the following model will be used. The cavity consists of two parallel and plane mirrors separated by the distance L. Each mirror is characterized by a field reflectivity coefficient r and a field transmission coefficient t. Also, the mirror has some losses described by the field loss coefficient l. From energy conservation this coefficient is connected to r and t by:

$$r^2 + t^2 + l^2 = 1.$$

A plane electromagnetic wave E_{in} enters the cavity from the left side, and part of the incoming field $t_1 E_{in}$ is transmitted through the first mirror. This field propagates to the second mirror and acquires a phase shift of $e^{-i\omega L/c}$ due to the propagation along the distance L. This field is partially transmitted through the second mirror ($E_{1tr} = t_1 t_2 E_{in} e^{-i\omega L/c}$) and partially reflected ($t_1 r_2 E_{in} e^{-i\omega L/c}$) and so on (see Fig. 1.1). The transmitted components interfere with each other. After summing up all the infinitely many components of the transmitted field

$$E_{tr} = E_{1tr} + E_{2tr} + ...$$

we obtain:

$$E_{tr} = E_{in} t_1 t_2 \sum_{k=0}^{\infty} r_1^k r_2^k e^{-i(2k+1)\omega L/c} = E_{in} t_1 t_2 e^{-i\omega L/c} \frac{1}{1 - r_1 r_2 e^{-2i\omega L/c}}. \qquad (1.1)$$

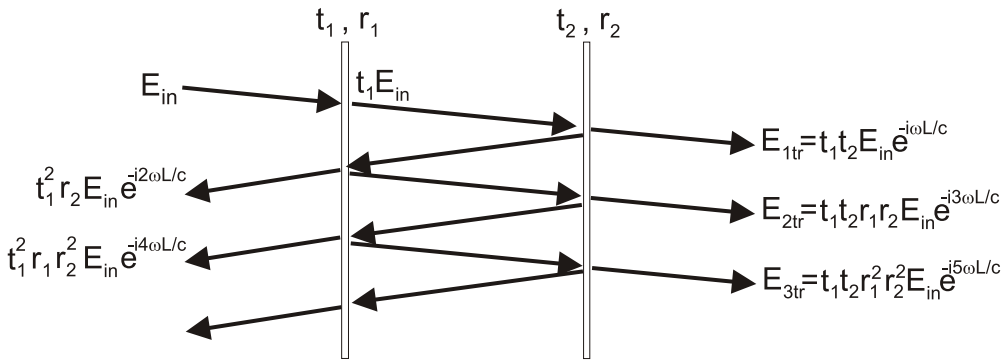

Figure 1.1: Model cavity that consists of two plane mirrors. Each mirror is characterized by a field reflection coefficient r and a field transmission t. Plane electromagnetic waves propagate between these mirrors.

The transmitted intensity is:

$$\frac{I_{tr}}{I_{in}} = \left|\frac{E_{tr}}{E_{in}}\right|^2 = \frac{t_1^2 t_2^2/(1-r_1 r_2)^2}{1+\frac{4r_1 r_2}{(1-r_1 r_2)^2}\sin^2(\frac{\omega L}{c})}. \tag{1.2}$$

This expression shows that the optical resonator exhibits a strong resonance behavior (see Fig. 1.2) each time the round-trip phase shift $2\omega L/c$ equals an integer multiple of 2π:

$$\omega = \omega_q = q \cdot 2\pi \frac{c}{2L}, \tag{1.3}$$

where q is an integer number. The frequency interval between two neighboring resonances is known as the *free spectral range* (FSR) of the cavity:

$$\omega_{FSR} = 2\pi \frac{c}{2L}. \tag{1.4}$$

Introducing the following definitions

$$F \equiv \frac{\pi\sqrt{r_1 r_2}}{1-r_1 r_2} \tag{1.5}$$

and

$$T_{max} \equiv \frac{t_1^2 t_2^2}{(1-r_1 r_2)^2}$$

we can write Eq. 1.2 in the following form:

$$\frac{I_{tr}}{I_{in}} = \frac{T_{max}}{1+\left(\frac{2F}{\pi}\right)^2 \sin^2(\frac{\pi\omega}{\omega_{FSR}})}. \tag{1.6}$$

Here, T_{max} is the maximum possible energy transmission.

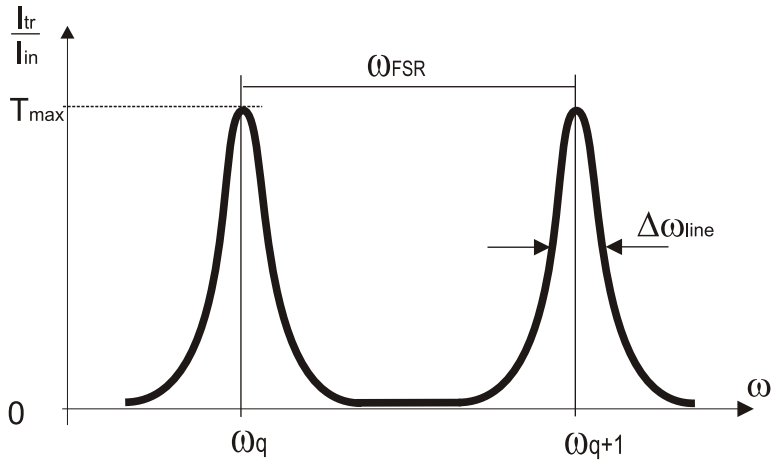

Figure 1.2: Cavity transmission versus frequency

The value F is called the *finesse* of the cavity. According to the definition of F its value depends only on the reflectivity of the mirrors and not on the distance between the mirrors. The finesse can be understood as the number of times a photon inside the cavity is reflected back and forth until it is finally transmitted through one of the mirrors.
The full width of the cavity transmission line, $\Delta\omega_{line}$, is defined by the condition that the transmitted intensity is reduced by the factor of 2:

$$\frac{I_{tr}}{I_{in}} = \frac{T_{max}}{2}$$

and therefore

$$\sin\left(\frac{\pi\Delta\omega_{line}/2}{\omega_{FSR}}\right) = \frac{\pi}{2F}.$$

The linewidth is approximately

$$\Delta\omega_{line} \simeq \frac{\omega_{FSR}}{F}. \tag{1.7}$$

The higher the finesse, the narrower are the transmission peaks with the same free spectral range.

1.1.2 Reflection

In the same way the field that is reflected from the cavity can be derived:

$$E_r = E_{in}\left(r_1 - r_2 t_1^2 e^{-2i\omega L/c}\frac{1}{1 - r_1 r_2 e^{-2i\omega L/c}}\right). \tag{1.8}$$

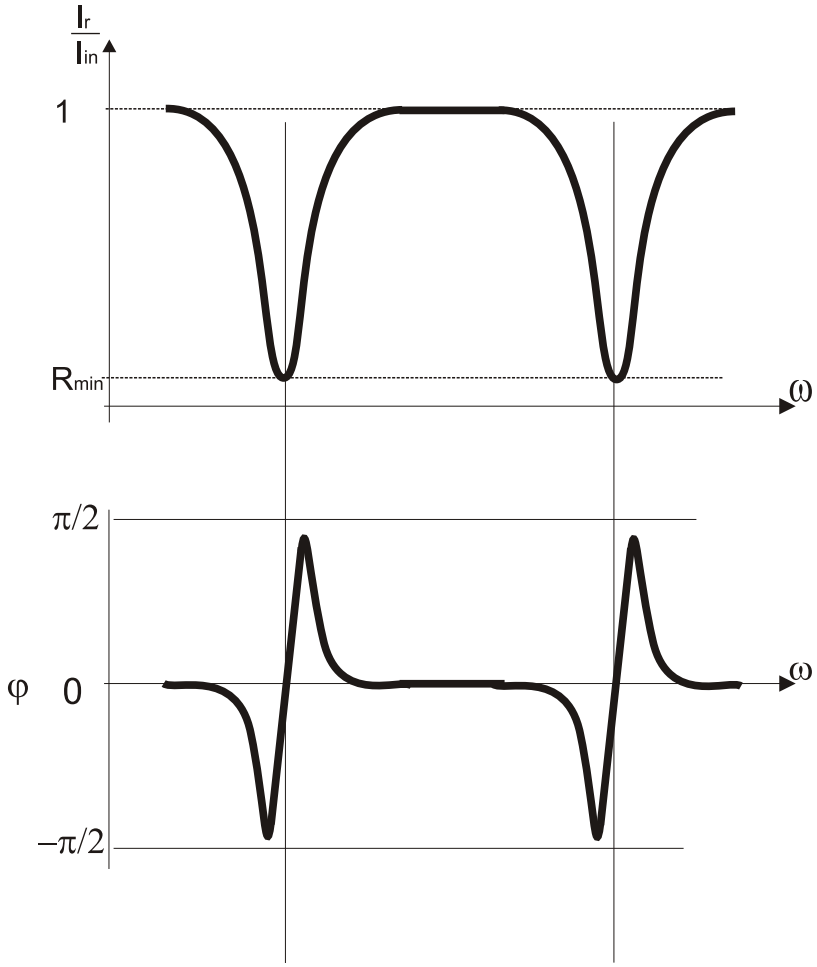

Figure 1.3: Reflected intensity and phase shift of the reflected signal versus frequency

The corresponding reflected intensity is calculated by squaring Eq. 1.8, which, for the case of resonance, yields

$$\left(\frac{I_r}{I_{in}}\right)_{res} = R_{min} = \left(\frac{r_1 - r_2}{1 - r_1 r_2}\right)^2 .$$

The phase of the reflected field is calculated from

$$\varphi = \arctan\left(\frac{Im(\frac{E_r}{E_{in}})}{Re(\frac{E_r}{E_{in}})}\right).$$

The behavior of the reflected intensity and of the phase of the reflected beam is presented in Fig. 1.3.

1.1.3 Intracavity field

In the same way the intracavity field is

$$E_{cr} = E_{in}\frac{t_1}{1 - r_1 r_2 e^{-2i\omega L/c}}. \tag{1.9}$$

The corresponding intensity in resonance for the case of equally high reflecting lossless mirrors, $r_1 = r_2 \simeq 1$, is

$$\left(\frac{I_{cr}}{I_{in}}\right)_{res} \simeq \frac{F}{\pi}. \tag{1.10}$$

Eq. 1.10 describes the intracavity intensity enhancement.

1.1.4 Gaussian beams

The propagation of the electromagnetic field is described by the Maxwell equations. For fields propagating along one direction, the z-direction, a *paraxial approximation* can be applied [Sie86]

$$E(x, y, z, t) = Re\left(u(x, z)v(y, z)e^{i\omega t - ikz}\right).$$

The solution of the wave equation in the paraxial approximation as a function of the z and x coordinates has the form

$$u_n(x, z) = c_n \left(\frac{\exp[i(2n+1)\psi(z)]}{2^n n! w(z)}\right)^{\frac{1}{2}} H_n\left(\frac{\sqrt{2}x}{w(z)}\right) \exp\left[-i\frac{kx^2}{2R(z)} - \frac{x^2}{w^2(z)}\right], \tag{1.11}$$

a set of Hermit-gaussian modes of different orders $n = 0, 1, ...,$
$H_n(x)$, - Hermitian polynomial of the n-th order,
z_R, - Rayleigh-range,
$w_0 = \sqrt{\frac{\lambda z_R}{\pi}}$, - beam waist,
$\lambda = 2\pi c/\omega$, - wavelength of the electromagnetic field,
$\psi(z) = \arctan\left(\frac{z}{z_R}\right)$, - Guoy-phase,
c_n, - normalization constant,

$$w(z) = w_0\sqrt{1 + \left(\frac{z}{z_R}\right)^2}, \text{ - beam radius,} \tag{1.12}$$

$$R(z) = z + \frac{z_R^2}{z}, \text{ - curvature of the wavefront.} \tag{1.13}$$

Analogously one can write an expression $v_m(y,z)$ for the y direction. The total Hermite-gaussian profile is given by the product

$$U_{n,m}(x,y,z) = u_n(x,z)v_m(y,z), \tag{1.14}$$

where m is the order of the transverse mode in y-direction.

The corresponding lowest order ($n = 0$, $m = 0$) electromagnetic wave that propagates along the z-axis is

$$E(x,y,z,t) = E_0 \frac{w_0}{w(z)} \exp\left(\frac{x^2+y^2}{w^2(z)}\right) \cos\left(-kz + \omega t - \frac{k\,(x^2+y^2)}{2R(z)} + \psi(z)\right), \tag{1.15}$$

where E_0 is the maximum of the field amplitude.

1.1.5 Higher transverse modes

Standing wave resonator

In the previous model of the optical resonator we assumed that the surfaces are plane, and the waves inside the cavity are plane waves.
Now assume the following model that a cavity consists of two spherical mirrors characterized by the parameters r and t of the reflecting surfaces at the distance L and, in addition, by radii of curvature of the mirrors, R. The mirrors are facing each other perpendicular to the z-axis at positions z_1 and z_2. If the radii of mirrors equal the radii of curvature of the wavefront of the gaussian beam at these points, the beam is reflected back into itself, and a standing wave is formed. For the lowest order of the Hermite-gaussian beam Eq. 1.15, the corresponding intensity distribution averaged over time is

$$I(x,y,z) = A\frac{1}{2}c\varepsilon_0\langle(E(x,y,z,t) + E(x,y,-z,t))^2\rangle$$

$$= I_0 \frac{w_0^2}{w^2(z)} \exp\left(\frac{2(x^2+y^2)}{w^2(z)}\right) \cos^2\left(-kz - \frac{k(x^2+y^2)}{2R(z)} + \psi(z)\right), \tag{1.16}$$

where A accounts for the resonant enhancement inside the cavity. The $\cos^2$ term shows that there are nodes and antinodes along the optical axis. The position of the antinodes satisfy:

$$kz - \psi(z) = q\pi, \tag{1.17}$$

where q is an integer number.

Guoy-phase

Now consider the consequences of factor $2n+1$ in the exponent $\exp[i(2n+1)\psi(z)]$ from Eq. 1.11. It results in different phase shifts for different transverse modes inside the cavity. The resonance condition for the cavity requires that the total round-trip phase shift is an integer multiple of 2π (the condition analogous to the condition in Eq. 1.3). Therefore, different transverse modes have different resonance frequencies (see Fig. 1.4).

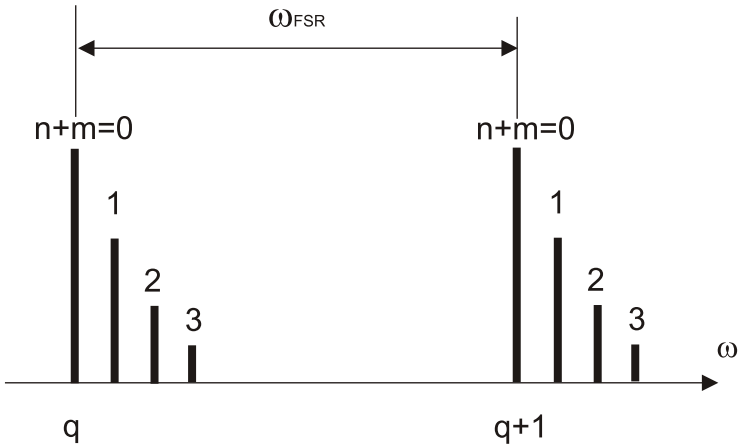

Figure 1.4: Cavity transverse modes

Eq. 1.3 can be generalized for higher transverse modes (see [SIE86]):

$$\omega = \omega_{qnm} = \left[q + (n+m+1)\frac{\psi(z_2) - \psi(z_1)}{\pi}\right]\frac{2\pi c}{2L}, \tag{1.18}$$

where z_1 and z_2 are the positions of the first and the second mirror, and

$$\psi(z_2) - \psi(z_1) = \arccos\left(\sqrt{\left(1 - \frac{L}{R_1}\right)\left(1 - \frac{L}{R_2}\right)}\right) \tag{1.19}$$

is the Guoy-phase phase shift, which lifts the degeneracy of the transversal modes.

1.2 Atom-cavity interaction

In this section the problem of the interaction of a two-level atom with the quantized electromagnetic field of the cavity mode is considered.

1.2.1 Harmonic oscillators

Many features of the quantum mechanical system of atom plus cavity can be found in the classical analogy of two equal harmonic oscillators (see Fig.1.5).
In the case of no coupling between the oscillators, the eigenmodes of the system are degenerate. If the oscillators are coupled by a spring with the coupling strength g_0, there is a coherent energy exchange between the oscillators, and the system has two nondegenerate eigenmodes.
Now assume that the oscillators have damping with rates κ and γ. If the coupling is smaller than the damping rates, the energy will be dissipated from the system before any coherent energy exchange takes place.

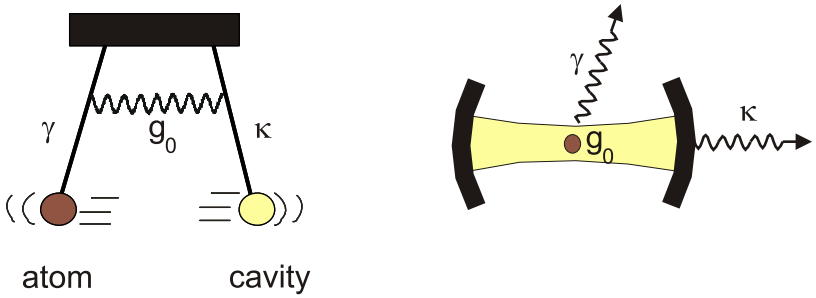

Figure 1.5: Left: two coupled harmonic oscillators with damping, right: system of an atom coupled to a cavity

Using this analogue, we proceed with the treatment of the quantum mechanical system of an atom coupled to a cavity.

1.2.2 Quantized cavity field and two-level atom

Now we consider the Jaynes-Cummings model [Jay63]: The cavity has only one field mode, it interacts with a two level atom, and there is no damping in the system. The corresponding Hamiltonian for the quantized cavity field is:

$$H_c = \hbar\omega_c a^+ a \tag{1.20}$$

and for the two-level atom:

$$H_a = \frac{1}{2}\hbar\omega_a\sigma_3, \tag{1.21}$$

where a and a^+ are the annihilation and creation operators for the cavity field; σ_3 is the Pauli matrix; ω_c and ω_a are the cavity and atomic resonance frequencies, respectively. Interaction between these systems, in the case of no damping, is described by the Hamiltonian

$$H_i = i\hbar\frac{g(\overrightarrow{r})}{2}(\sigma_+ a - a^+\sigma_-), \tag{1.22}$$

where σ_- and σ_+ are the atomic lowering and rising operators. The coupling constant, $g(\overrightarrow{r})$, between the atom and the cavity mode is expressed by

$$g(\overrightarrow{r}) = g_0 f(\overrightarrow{r}), \tag{1.23}$$

where $f(\overrightarrow{r})$ is the spatially dependent cavity mode function, g_0 is the maximum coupling constant.

Vacuum Rabi splitting

Consider the case of a cavity that is resonant with the atomic transition.
In the case of no interaction, the excited energy levels of the atom-cavity system are degenerate (see Fig. 1.6).

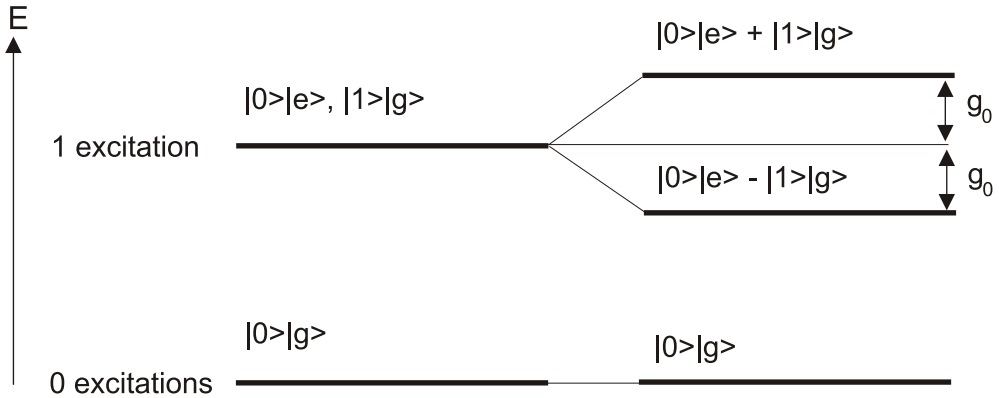

Figure 1.6: Transition from the uncoupled to the coupled atom-cavity system

In the presence of an interaction, the atom feels the presence of the cavity even if there are no excitations in the cavity mode. The states that correspond to one excitation in the system are mixed, and the degeneracy is lifted (see Fig. 1.6). This energy splitting is called *vacuum Rabi splitting*. As for the case of classical harmonic oscillators, a coherent energy exchange between the cavity mode and the atom takes place, and the system has two nondegenerate eigenmodes.

Strong coupling

Let us introduce damping into this system (see Fig. 1.5): the cavity energy decay rate, $\kappa \equiv \Delta\omega_{line}$, and the spontaneous decay rate of atom, γ, from the excited state into modes other than the cavity mode. Analogously to the classical harmonic oscillators system, the atom and the cavity field mode coherently exchange energy, if the damping is lower than the coupling g_0. The condition

$$g_0 \geq \gamma, \kappa \tag{1.24}$$

is known in cavity QED as the condition of *strong coupling*.

In the frequency domain the damping will result in the broadening of lines (Fig. 1.7). In the regime of strong coupling the separation between the two lines will be larger than the width of each line.

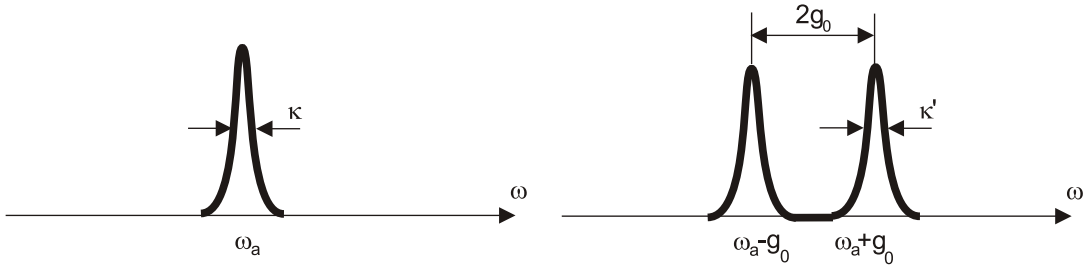

Figure 1.7: Cavity transmission spectrum, transition from the uncoupled to the coupled atom-cavity system. κ' is a function of κ, γ, g_0.

To have a quantitative picture of the vacuum Rabi splitting, an explicit expression for the interaction constant $g(\overrightarrow{r}) = f(\overrightarrow{r})g_0$ will be derived.

Cavity mode function

For the case of a near planar cavity, $R \gg L$, the Rayleigh range can be approximated by

$$z_R^2 = \frac{LR}{2}\left(1 + \frac{L}{2R}\right) \simeq \frac{LR}{2}. \tag{1.25}$$

Therefore, the radius of the cavity mode at the mirror (1.12) roughly equals the waist:

$$w\left(\frac{L}{2}\right) = w_0\sqrt{1 + \frac{L}{2R}} \simeq w_0. \tag{1.26}$$

Applying this approximation to Eq. 1.15 and neglecting the change in curvature of the wavefronts, we get for the spatially dependent cavity mode function

$$f(\overrightarrow{r}) = \exp\left(-\frac{(x^2+y^2)}{w_0}\right)\cos\left(\frac{\pi}{L}z\right). \tag{1.27}$$

Coupling constant

The goal of this section is to calculate the coupling constant g_0 as a function of cavity and atomic parameters.
By definition, $g(\overrightarrow{r})$ is the interaction rate between an atom and the field of the cavity mode

$$\hbar g(\overrightarrow{r}) = \overrightarrow{d} \cdot \overrightarrow{E}(\overrightarrow{r}), \tag{1.28}$$

where $d = |\overrightarrow{d}|$ is the dipole moment of the atomic transition, $E(\overrightarrow{r}) = |\overrightarrow{E}(\overrightarrow{r})| = E_0 f(\overrightarrow{r})$ is the electric field amplitude of the cavity mode, E_0 is the maximum amplitude of the cavity field.

The expression for E_0 can be derived from the requirement that the energy of the field mode is the zero-point energy

$$\frac{\hbar\omega_c}{2} = \varepsilon_0 E_0^2 \int_{mode} [f(\overrightarrow{r})]^2 \, dV, \tag{1.29}$$

Integration of Eq. 1.29 using Eq. 1.27 yields

$$E_0 = \left(\frac{\hbar\omega_c}{2\varepsilon_0 V}\right)^{\frac{1}{2}}, \tag{1.30}$$

with the cavity mode volume

$$V = \int_{mode} [f(\overrightarrow{r})]^2 \, dV = \frac{\pi w_0^2 L}{4}. \tag{1.31}$$

This gives the following expression for g_0

$$g_0 = \sqrt{\frac{d^2\omega_c}{2\hbar\varepsilon_0 V}}. \tag{1.32}$$

The coupling constant g_0 is a function of the atomic parameters d and ω_c, and of the cavity parameter V. For a given atom, the coupling constant can be increased by minimizing the cavity mode volume. The cavity mode volume can be decreased by minimizing the length of the cavity and the radii of curvature of the mirrors.

Chapter 2

Microcavities

The main requirement for a cavity for CQED experiments with single atoms is the possibility to reach the regime of strong coupling. A high coupling constant g_0 requires the separation between the cavity mirrors to be as small as possible. In the specific case of our setup the lower limit is set by the condition that the dipole trap laser must fit between the mirrors without creating stray light. With the waist of this laser being 20 μm the cavity mirror spacing should be about 200 μm. Second, a low cavity decay rate κ requires a high finesse.

The construction of a high finesse cavity is the aim of this work. In this chapter I will describe the characteristics of highly reflecting mirrors, the construction and the characterization of the cavity.

2.1 Mirrors

As was mentioned in the previous chapter, the cavity mirrors must have an extremely high reflectivity to guarantee a high finesse of the cavity. Besides, the cavity mirrors must have a special shape and size because the cavity has to be integrated into the existing setup. The mirrors were manufactured by the company Research Electro-Optics (REO, Boulder, CO, USA). The mirror substrate is a quartz cylinder with a cone-shaped side (see Fig. 2.1).

The mirror surface has a diameter of 1 mm and a radius of curvature of 1 cm. We ordered two types of mirrors: one charge with a very high reflectivity of 99.997 %, and a second charge with a slightly lower reflectivity of 99.994 % at 852 nm. The other side of the mirror has an anti-reflection coating, with a specified reflectivity of 0.02 %.

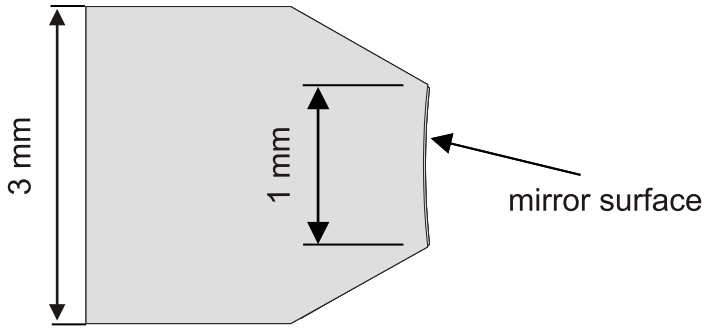

Figure 2.1: Cavity mirror

2.2 PZTs

The mirrors are glued onto shear Piezo Translators (PZTs), which are used to scan the length of the cavity. The application of a high voltage causes the surfaces of a shear PZT to shift relative to each other (see Fig. 2.2).

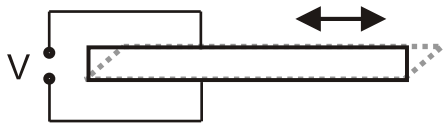

Figure 2.2: Shear PZT

Our PZTs are produced by the company PI-Ceramic, and have a squared shape (6 mm $\times$ 6 mm) and a thickness of 1 mm. The surfaces are Au-coated to provide electrical contacts. A maximum voltage up to ± 500 V can be applied to shift the surfaces of the PZT by ± 300 nm, which is enough to scan $1 - 2$ FSR.

2.3 Construction of the cavity

The construction of the cavity (Fig. 2.3) is done in the following way. All the manipulations are done in dust free environment - under a flow box.

- *Preparation of mirrors*

  It was observed that all mirrors have dust particles or small pieces of glass on the surface, some mirrors additionally have scratches. Two mirrors that do not have scratches are selected. The dust and the glass pieces are removed using a special polymer called "Opticlean" in the following way. The mirror is placed into the mirror holder (see Fig. 2.4). A droplet of Opticlean is placed exactly in the center of the mirror. A sheet of lens cleaning tissue is placed on top of this droplet. An additional droplet of Opticlean is placed on top. After about

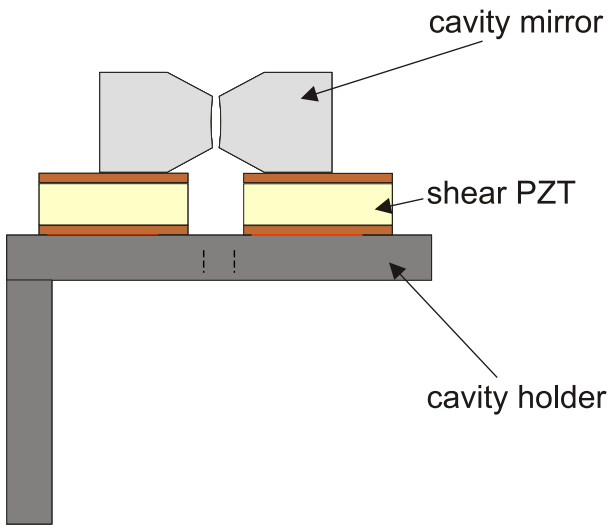

Figure 2.3: Scheme of the cavity

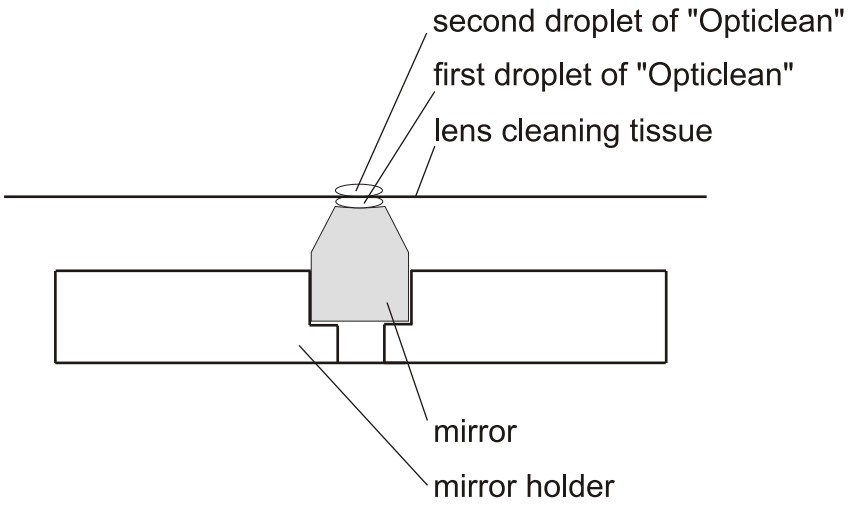

Figure 2.4: Cleaning the cavity mirrors with Opticlean

20 minutes the tissue with the Opticlean is removed. The mirror is examined under a microscope with 100 x magnification. Usually it was sufficient to clean the mirror $2-5$ times to get rid of all dust particles and glass pieces.

- *Preparation of the cavity holder*

  The PZTs are fixed to the cavity holder using a vacuum compatible glue (EPO-TEK 353ND, Polytec). To get rid of the residual air dissolved in the glue, it has to be degassed in an evacuated environment for about 5 hours. The PZTs are positioned and glued. Then the glue is baked in an evacuated oven for

two hours at a temperature of 150 °C to harden. The glue layer between the aluminum cavity holder and the Au-layer of the PZT is so thin that there is still an electrical contact.

- *Fixing the mirrors*

  The mirrors are positioned and centered using a special mirror positioning V-groove tool (see Fig.2.5). This V-groove automatically centers the cylindrical

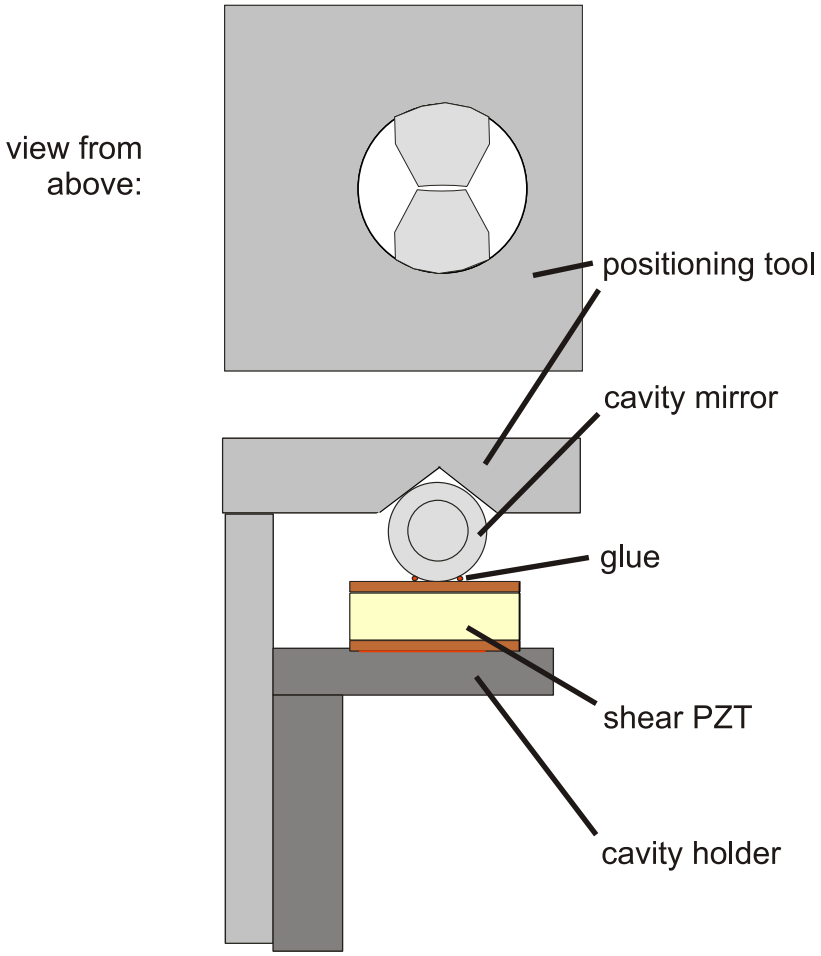

Figure 2.5: V-groove positioning tool for centering the mirrors

substrates of the mirrors. The hole at the top of the V-groove allows us to look at the mirrors from above through a microscope to adjust the distance between the mirrors to about 200 μm. Then the V-groove is fixed, and the mirrors are glued at two points. The cavity is baked again for two hours at a temperature of 150 °C to harden the glue.

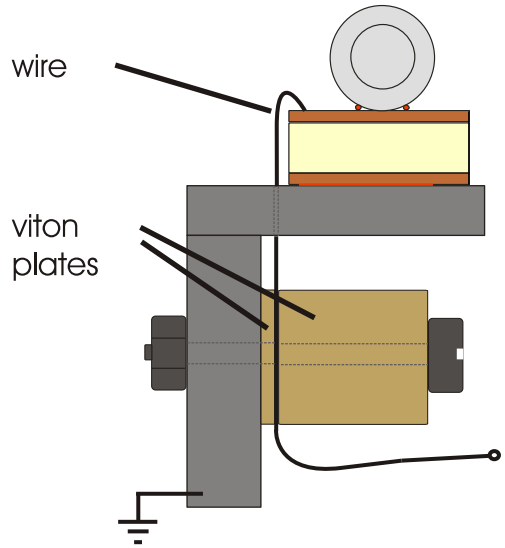

Figure 2.6: A capton-isolated wire is clamped with two viton plates

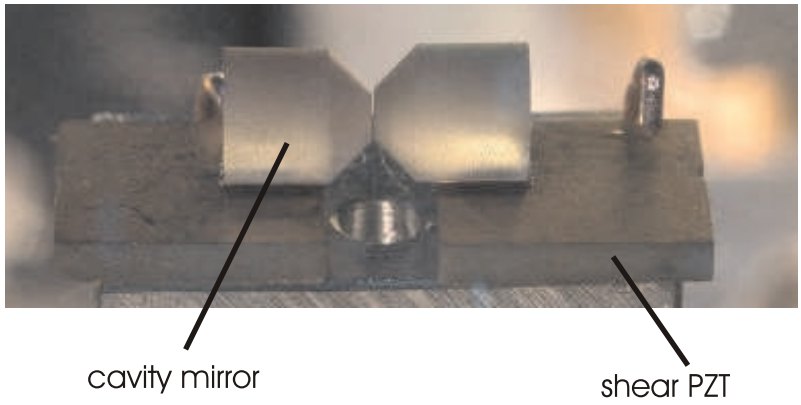

Figure 2.7: Assembled high finesse cavity

- *Connecting PZT contacts*

  The final step in the construction of the cavity is to connect the PZT contacts. The bottom side of the PZT is connected through the cavity holder to the ground. The top contact of the PZT is connected with a wire. For vacuum compatibility reasons we use a special capton-isolated wire and clamp it with two viton plates (see Fig.2.6).

The cavity is now ready for tests. Fig. 2.7 shows a photo of a real cavity. The first cavities were tested and characterized on air without placing them into a vacuum chamber.

2.4 Characterization of the cavity

This section covers the measurement of the cavity parameters, such as the length and the finesse of the cavity. Since we couple two lasers into the cavity (a probe-laser at 852 nm and a lock-laser at 836 nm, see Chapter 4), these parameters were measured for these two wavelengths.

2.4.1 Setup

The setup for the characterization of the cavity is presented in Fig. 2.8. Light from the laser is sent through the Acousto-optical modulator (AOM) and then into the fiber. The AOM is used for the calibration of the transmission spectrum of the cavity (see the next subsection). The fiber works as a mode cleaner, which transforms the beam that comes out of the diode laser into a gaussian beam. The telescope (see Fig. 2.9) is used for mode matching of the cavity. The transmitted light after the

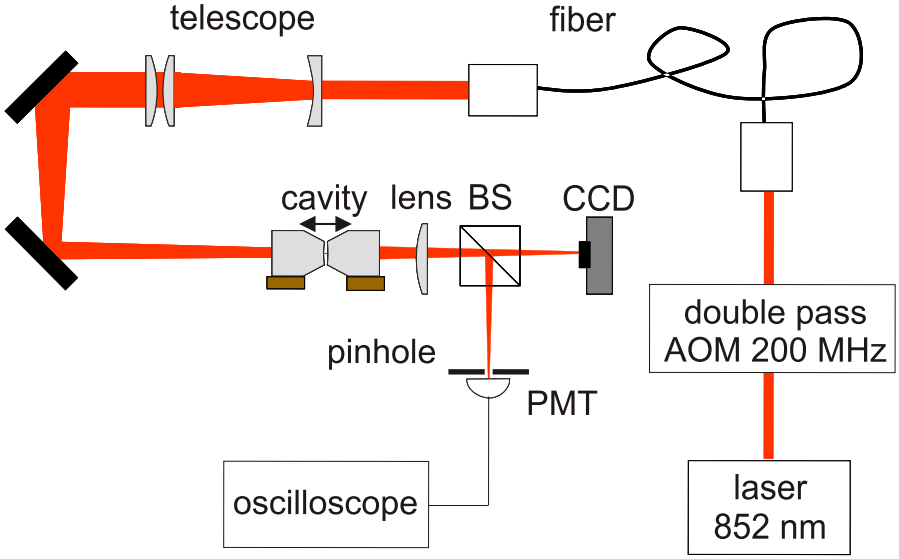

Figure 2.8: Setup for characterization of the cavity

cavity is focused with the lens and is split by the beam splitter BS. Part of the light is sent onto the CCD camera to observe the cavity modes. More important, the other part of the light is sent through a 90 μm pinhole onto the Photomultiplier Tube (PMT). This spatial filtering before the PMT is necessary to filter out the light that is scattered by the fiber out-coupler objective, by the telescope lenses and by the coupling mirrors.
We record the transmission spectrum of the cavity as a function of voltage applied to the PZTs (see Fig. 2.10). The parameters of the cavity are extracted from the transmission spectrum.

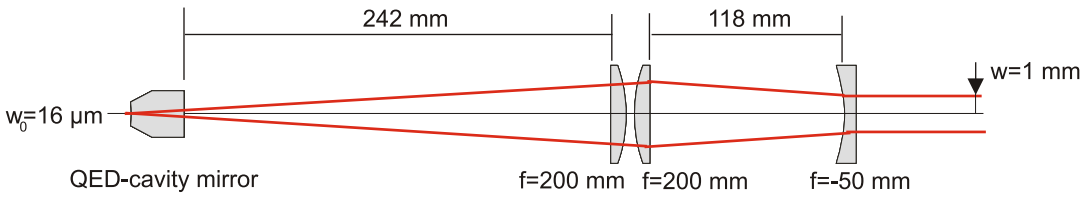

Figure 2.9: Telescope for mode matching of the QED-cavity. Aberrations at the position of the cavity mode are smaller than the diffraction limit.

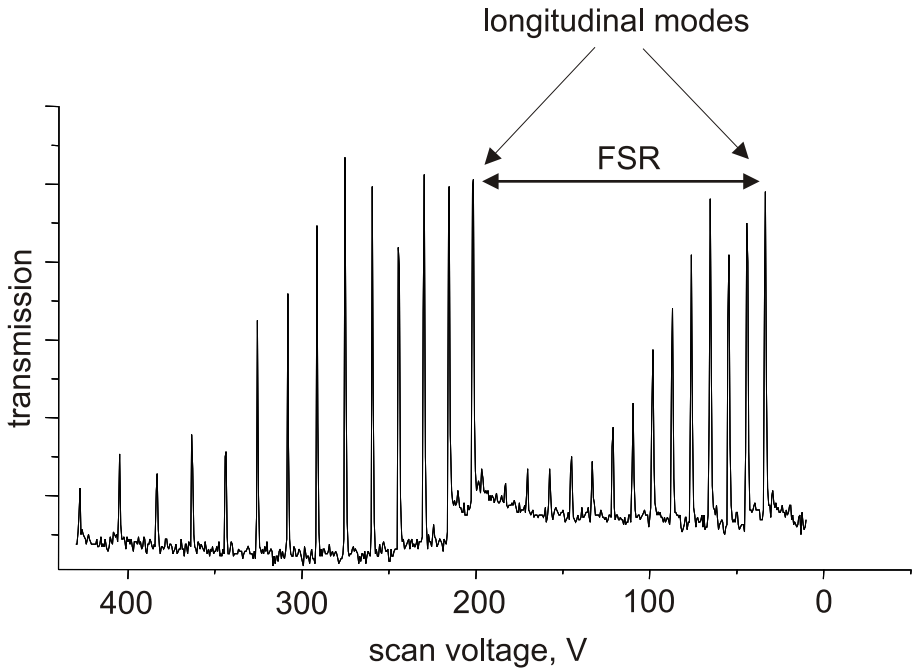

Figure 2.10: Recorded transmission spectrum of the cavity

2.4.2 Principle of the measurement

The goal of this section is to show how the length and finesse of the cavity can be extracted from the transmission spectrum.

We measure the linewidth of the cavity TEM_{00} mode, ν_{line}, and the distance between the two neighboring transversal modes, $\Delta\nu_{transv}$. From the distance between the two neighboring transversal modes and the radius of curvature of the mirrors, $R = 1$ cm, we calculate the length, L, of the cavity using the formula (see Eq. 1.18):

$$\Delta\nu_{transv} = \frac{\arccos(1 - \frac{L}{R})}{\pi} \frac{c}{2L}. \tag{2.1}$$

For the case $L \ll R$, the following approximation can be applied

$$\arccos(1-x) \simeq \sqrt{2}\sqrt{x} + O(x^{\frac{3}{2}}).$$

Eq. 2.1 simplifies to

$$L = \frac{2c^2}{(2\pi\Delta\nu_{transv})^2 R}. \tag{2.2}$$

From the length of the cavity we calculate the FSR of the cavity (see Eq. 1.4)

$$\nu_{FSR} = \frac{c}{2L}.$$

And, finally, we get the finesse of the cavity (see Eq. 1.7)

$$F = \frac{\nu_{FSR}}{\nu_{line}}. \tag{2.3}$$

2.4.3 Measurement of the cavity parameters

Linewidth

The cavity is scanned by applying a DC offset to one of the PZTs and scanning the other PZT by the signal derived directly from the function generator without any high voltage amplifier. The transmission spectrum (see Fig. 2.11) was recorded by triggering the storage scope to the top of the line and averaging 64 times. We use an AOM in double pass configuration, in order to calibrate the transmission spectrum. The AOM produces a sideband 200 MHz away from the carrier frequency. The zeroth and first order of the AOM are simultaneously coupled to the fiber and sent into the cavity. Using this calibration we determine the width of the TEM_{00} line of the cavity to be

$$\nu_{line} = 7.1\ MHz.$$

This value of the linewidth is an upper limit of the real value, because the measured linewidth contains a set of systematic errors: acoustical vibrations, triggering error, nonlinearity of PZTs, electrical noise, the finite line width of the probe laser, the noise from electronics. The total error was estimated to be of the order of 5% mainly due to the acoustical vibrations, because no special acoustical shielding of the cavity was used - the holder of the cavity was directly fixed to the optical table.

The linewidth of the laser has to be smaller than the linewidth of the cavity, in order to perform the measurement of the linewidth of the cavity. In time domain, the coherence time of the laser should be longer than the cavity decay time. Detecting the beat signal between the 852 nm probe laser and a master laser, we have measured the linewidth of the probe laser to be about 100 kHz. This value is few orders of magnitude smaller than the measured linewidth of the cavity.

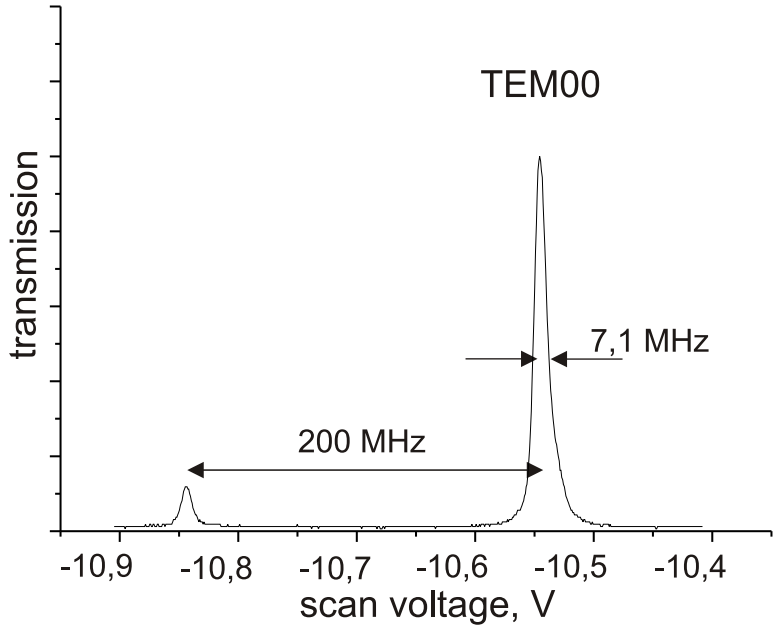

Figure 2.11: TEM00 mode and the 200 MHz side band

Distance between transversal modes

This measurement was done by recording a spectrum with a few transversal modes. The calibration from the measurement of the linewidth was used to calculate the distance between the two neighboring transversal modes, $\Delta\nu_{transv} = 40$ GHz, (see Fig. 2.12). Here the error was estimated to be about 5% mainly due to the nonlinearity of the PZTs.

The length of the cavity was determined using formula (2.2):

$$L = (270 \pm 20)\ \mu m.$$

Consequently, $\nu_{FSR} = (540 \pm 50)$ GHz and the finesse of the cavity is

$$F = 77000 \pm 8000.$$

2.5 Discussion

During this work I have built and characterized several cavities: One asymmetric cavity, with two different mirrors of 99.997% and 99.994% reflectivity, and two symmetric cavities, with both 99.997% reflectivity mirrors. The cavity parameters were measured for two linewidths, 852 nm and 836 nm (see Fig 2.13). The measured finesse (the error is about 10%) was slightly less than the expected specified value.

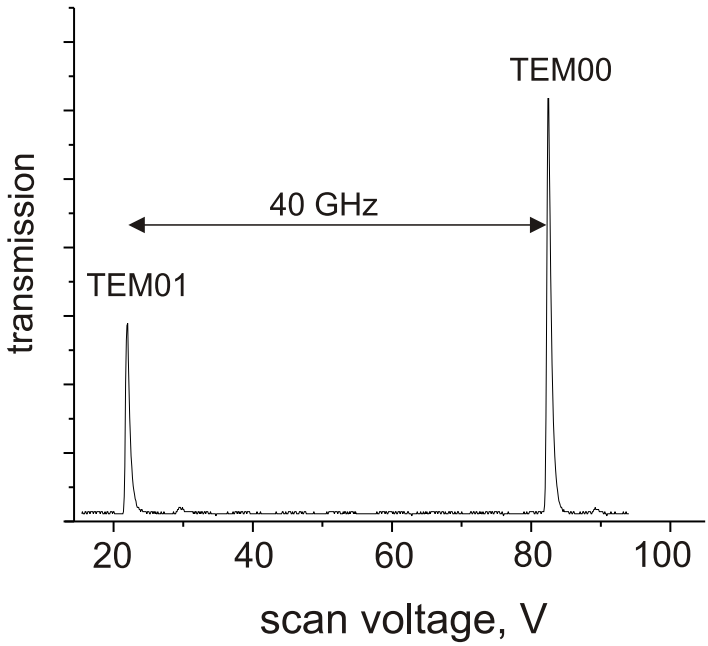

Figure 2.12: TEM00 and TEM01 transversal modes

	L, μm	852 nm F	852 nm F_{spec}	836 nm F	$(\frac{\kappa}{2\pi}, \frac{g_0}{2\pi}, \frac{\gamma}{2\pi})$MHz
cavity 1 (asymm.)	40	80000	69000		(23, 42, 5)
cavity 2 (symm.)	260	94000	104000	78000	(3.1, 10.5, 5.2)
cavity 3 (symm.)	270	77000	104000	52000	(3.6, 10.1, 5.2)

Figure 2.13:

Other groups, who use the same mirrors, achieved a finesse of about 300000. We are currently optimizing the cleaning methods of the mirrors. This could allow us to achieve a higher finesse.

Nevertheless, even the current parameters of the cavities already allow us to achieve the regime of strong coupling:

$$(g_0, \kappa, \gamma) = 2\pi \cdot (10, 3, 5) MHz.$$

Chapter 3

Laser-cavity stabilization

The goal of the experiment is to obtain controlled interaction of single atoms with single photons stored in a cavity. This requires that the cavity resonance frequency should be stabilized to the atomic resonance.
Acoustic vibrations and thermal drifts are the two main factors that can change the distance between the mirrors of the cavity in an uncontrollable way. For the case of a high finesse cavity ($F = 100000$ at 852 nm), a change of 0.5 pm in length already shifts cavity resonance by one linewidth. So, the passive stability of the cavity does not suffice for our experiments with controlled atom-photon interaction. That is why an active compensation of these jitters and drifts is necessary. We use a stable narrow linewidth laser to stabilize the length of the cavity.

3.1 Active cavity stabilization

The idea of cavity length stabilization is simple in principle: one has to detect the direction and the amplitude of the deviation of the cavity length from a required value (get an error signal) and, based on this error signal, produce and send a corresponding voltage to the cavity PZTs to compensate the deviation. So, a key point of the active stabilization is to produce an error signal that has the following properties: it has to be zero if the cavity length has a required value, and it has to have different signs depending on the direction of the deviation of the length of the cavity.

There are several methods to produce an error signal from a cavity and, therefore, to realize a laser-cavity stabilization. One possibility is to use the reflection of the cavity (see Fig. 3.1). The phase change of the reflected beam has the necessary dispersive shape around the resonance. We use the Pound-Drever-Hall method [Dre83] to detect the phase and produce the error signal.

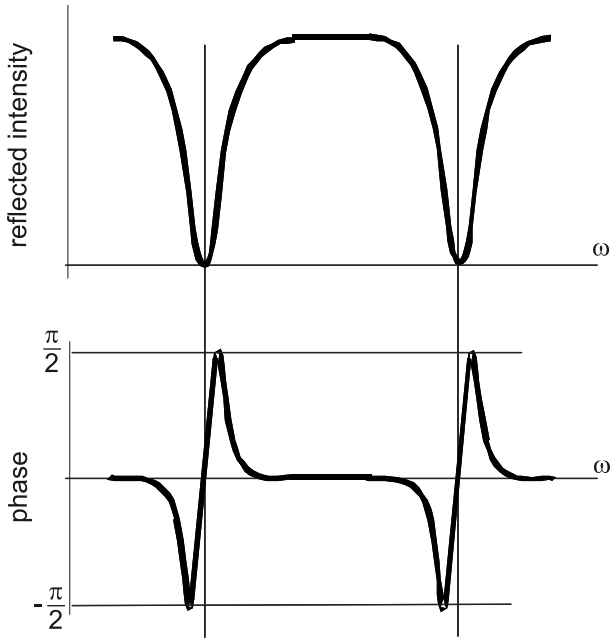

Figure 3.1: The reflected intensity has a Lorentzian lineshape, the phase has a dispersive lineshape

3.2 Pound-Drever-Hall method

The idea of this method can be explained in the following way. The phase of the reflected beam is compared to some known reference phase. For this purpose one phase modulates a laser beam with a frequency Ω that is larger than the cavity linewidth. This produces two sidebands around the laser carrier frequency ω_c (see Fig. 3.2). Since the sidebands are far away from the cavity resonance, they acquire no phase shift when reflected from the cavity. These sidebands are necessary to act as a reference for phase measurement of the carrier. The mechanism of the phase detection can be understood from the following example.

We consider the electric field of the carrier as a vector that rotates with the optical frequency ω_c in phase space. The corresponding sidebands are represented as vectors that rotate with the frequencies $\omega_c - \Omega$ and $\omega_c + \Omega$ in this phase space (see Fig. 3.3). In a frame of reference which rotates with the frequency ω_c the carrier is stationary, and the sidebands rotate with the frequencies Ω but in opposite directions. Due to the nature of the phase modulation the second sideband gets an additional π-phase shift - this fact is indicated in Fig. 3.3 by different directions of the sidebands. We reflect the beam with the three frequency components from the cavity. The left part of Fig. 3.6 shows the beam after the reflection. Let us consider three

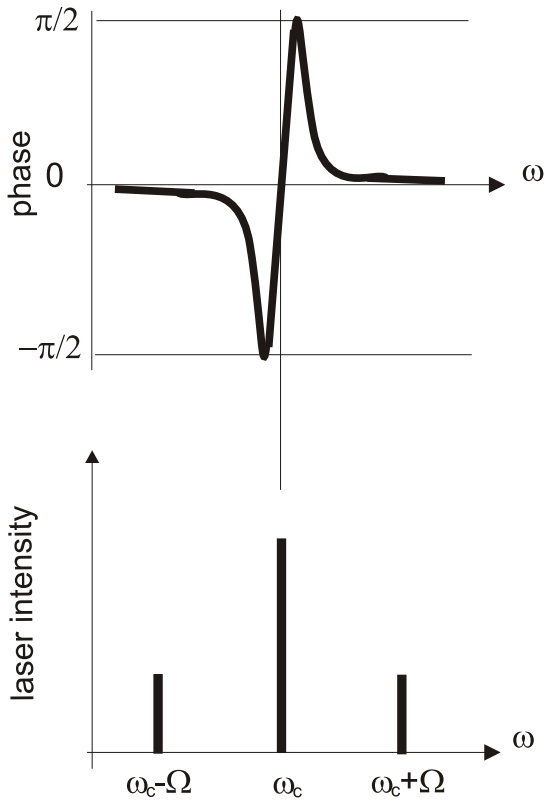

Figure 3.2: Laser carrier and sidebands

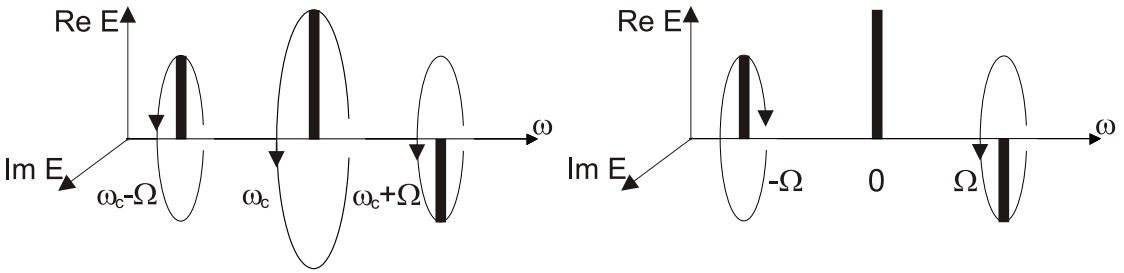

Figure 3.3: Left: the laser carrier and the sidebands in phase space. Right: the same, but in the rotating frame of reference

situations: when the cavity length has a necessary resonant value, when the cavity length is larger than the resonant value and when the cavity length is smaller than the resonant value.

If the cavity is held on resonance, the carrier, in the case of impedance matching, is not reflected, and one has only two reflected sidebands (see Fig. 3.6a). The central part of Fig. 3.6a presents the corresponding rotating electric field vectors. Two reflected beams interfere with each other. The resulting intensity oscillates with the

frequency 2Ω. This intensity can be detected by a photodiode (the right part of Fig. 3.6a). Now we take a reference sine wave, the same one as was used for the phase modulation of the beam. The overlap integral of this signal with the signal from the photodiode gives zero, as was expected for the resonance case.
If the cavity is held below resonance, the carrier is partially reflected (see Fig. 3.6b). Now three beams interfere with each other, and the corresponding intensity oscillates with the frequency Ω. The overlap integral of this signal with the reference sine wave at frequency Ω gives a positive value.
If the cavity is held above resonance (see Fig. 3.6c), the corresponding overlap integral gives a negative value.
Therefore, one can distinguish between different directions of the deviation of the cavity length. Now one can feed back to the PZTs the detected information about the cavity length deviation and compensate it.

The servo bandwidth of the Pound-Drever-Hall method is limited by the modulation frequency. One needs at least one cycle of the local oscillator to evaluate the overlap integral between the reference sine wave and the signal from the photo diode (see Fig. 3.6). So, all the jitters faster than the modulation frequency Ω cannot be detected and fed back to the system.

3.3 Implementation of the Pound-Drever-Hall method

In practice this scheme is realized in the following way (see Fig. 3.4). A local oscillator with frequency Ω is used to modulate the phase of the laser beam and acts as a reference signal. The photodiode detects the beat signal between the carrier and the sidebands. This signal is mixed with the signal from the local oscillator. After filtering out the high frequencies, one gets the necessary dispersive signal with zero crossing at the position of the carrier frequency (see Appendix A for PDH electronic circuits). Now let us follow these steps quantitatively.

- *Phase modulation*
  The laser light is phase-modulated with the frequency Ω. The electric field of the laser beam looks like

  $$E(t) = E_0 \sin(\omega t + \varphi(t)),$$

  where the phase modulation is

  $$\varphi(t) = \varepsilon \cdot \sin(\Omega t).$$

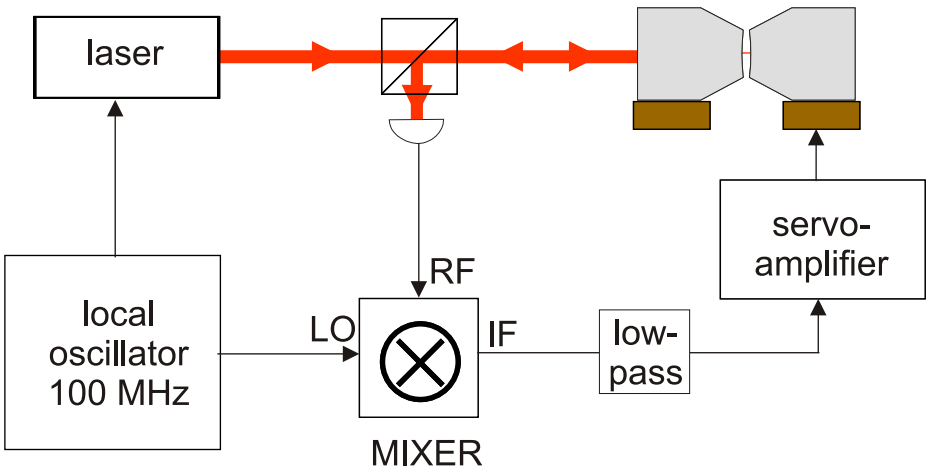

Figure 3.4: Implementation of the PDH method

The expression for the phase-modulated field for the case of weak modulation ($\varepsilon \ll 1$) can be approximated using the first three Bessel functions

$$E(t) \simeq E_0[J_{-1}(\varepsilon)\sin((\omega-\Omega)t) + J_0(\varepsilon)\sin(\omega t) + J_1(\varepsilon)\sin((\omega+\Omega)t)],$$

where $J_{-1}(\varepsilon) = -J_1(\varepsilon)$.

In practice it means that the laser field contains infinitely many frequency components, but only three of them are considerably big and produce observable effects.

This light field is reflected from the cavity. In general, every frequency component will have some change in amplitude and some phase shift. The reflected field is

$$\begin{aligned} E_{refl}(t) = E_0[&-A(\varepsilon,\Delta\omega)\sin((\omega-\Omega)t + \varphi_a(\varepsilon,\Delta\omega)) + \\ &+B(\varepsilon,\Delta\omega)\sin(\omega t + \varphi_b(\varepsilon,\Delta\omega)) + \\ &+A(\varepsilon,\Delta\omega)\sin((\omega+\Omega)t + \varphi_c(\varepsilon,\Delta\omega)), \end{aligned}$$

where B is the amplitude of the reflected carrier and A is the amplitude of the reflected sideband. $\varphi_{a,b,c}$ are the phase shifts for the corresponding components after the reflection. The amplitudes and the phases of the corresponding frequency components are functions of the modulation amplitude ε and the deviation $\Delta\omega$ of the cavity resonance frequency from the laser carrier frequency ω.

- *Reflected intensity*
  The resulting intensity of the reflected signal is

$$I \sim [-\sin(a) + \alpha \cdot \sin(b) + \sin(c)]^2$$

where $a = (\omega - \Omega)t + \varphi_a(\varepsilon, \Delta\omega)$, $b = \omega t + \varphi_b(\varepsilon, \Delta\omega)$, $c = (\omega + \Omega)t + \varphi_c(\varepsilon, \Delta\omega)$, $\alpha = B(\varepsilon, \Delta\omega)/A(\varepsilon, \Delta\omega)$. Detecting this signal with a photodiode effectively time averages this intensity over the carrier frequency ω:

$$I_{RF} = \langle I \rangle_t \sim \left(\frac{1}{2} + \alpha^2\frac{1}{2} + \frac{1}{2}\right) + 2\alpha \cdot \cos(b-c) - 2\alpha \cdot \cos(b-a) - 2\cos(c-a) =$$

$$= \left(1 + \frac{\alpha^2}{2}\right) + 2\alpha \cdot \cos(\varphi_b - \varphi_c - \Omega t) - 2\alpha \cdot \cos(\Omega t + \varphi_b - \varphi_a) - 2\cos(2\Omega t + \varphi_c - \varphi_a).$$

The terms with the phase φ_b, which we want to detect, oscillate with the frequency of the local oscillator Ω. To get rid of this oscillation, we beat I_{RF} with the local oscillator signal.

- *Mixing with local oscillator*
  For this purpose I_{RF} is fed into the RF port of the mixer and the signal from the reference local oscillator is fed into the LO port of the mixer:

  $$I_{RF} \cdot LO = I_{RF}(t) \cdot \sin(\Omega t)$$

  In practice, there has to be an additional phase shifter between the local oscillator and the LO-port of the mixer (see Fig. 3.4) to compensate the constant phase shift of the reference signal due to the elements of the circuit.

  This mixing will produce signals at the sum and difference frequencies. We filter out the high frequencies Ω, 2Ω and 3Ω, because we are interested only in the terms close to DC.

  $$I_{RF} \cdot LO \to \alpha \cdot \sin\varphi_b\,(\cos\varphi_c + \cos\varphi_a) - \alpha \cdot \cos\varphi_b\,(\sin\varphi_c + \sin\varphi_a)\,. \qquad (3.1)$$

  Let us assume that the modulation frequency is larger than the cavity linewidth. Then the sidebands acquire no phase shift after the reflection, $\varphi_a = \varphi_c = 0$, and the only phase sensitive to cavity length jitters is φ_b. So one has

  $$I_{RF} \cdot LO \to \alpha(\varepsilon, \Delta\omega) \cdot \sin\left(\varphi_b(\varepsilon, \Delta\omega)\right).$$

  One recalls that $\alpha = B(\varepsilon, \Delta\omega)/A(\varepsilon, \Delta\omega)$, where B is the amplitude of the reflected carrier and A is the amplitude of the reflected sideband. Because the modulation frequency is larger than the cavity linewidth, the sidebands do not change their amplitude even if the cavity drifts. Therefore, one has

  $$I_{RF} \cdot LO \to B(\varepsilon, \Delta\omega) \cdot \sin\left(\varphi_b(\varepsilon, \Delta\omega)\right). \qquad (3.2)$$

The behavior of B and φ_b as functions of frequency is presented in Fig. 3.1. This yields the total behavior of the $I_{RF} \cdot LO$-signal to be as presented in Fig. 3.5. So, using the PDH method, we produced a signal that contains the necessary phase information, and, consequently, this signal is an error signal.

The applications of the PDH method are versatile. Two of these are used in the experiment to stabilize two cavities and a laser (see the next chapter).

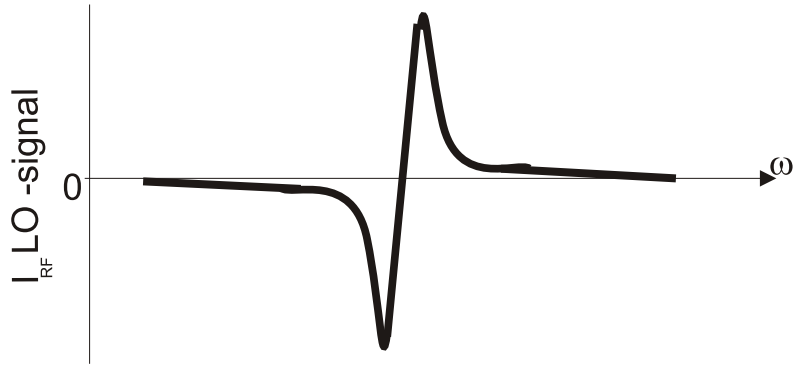

Figure 3.5: The $I_{RF} \cdot LO$-signal has a necessary dispersive shape

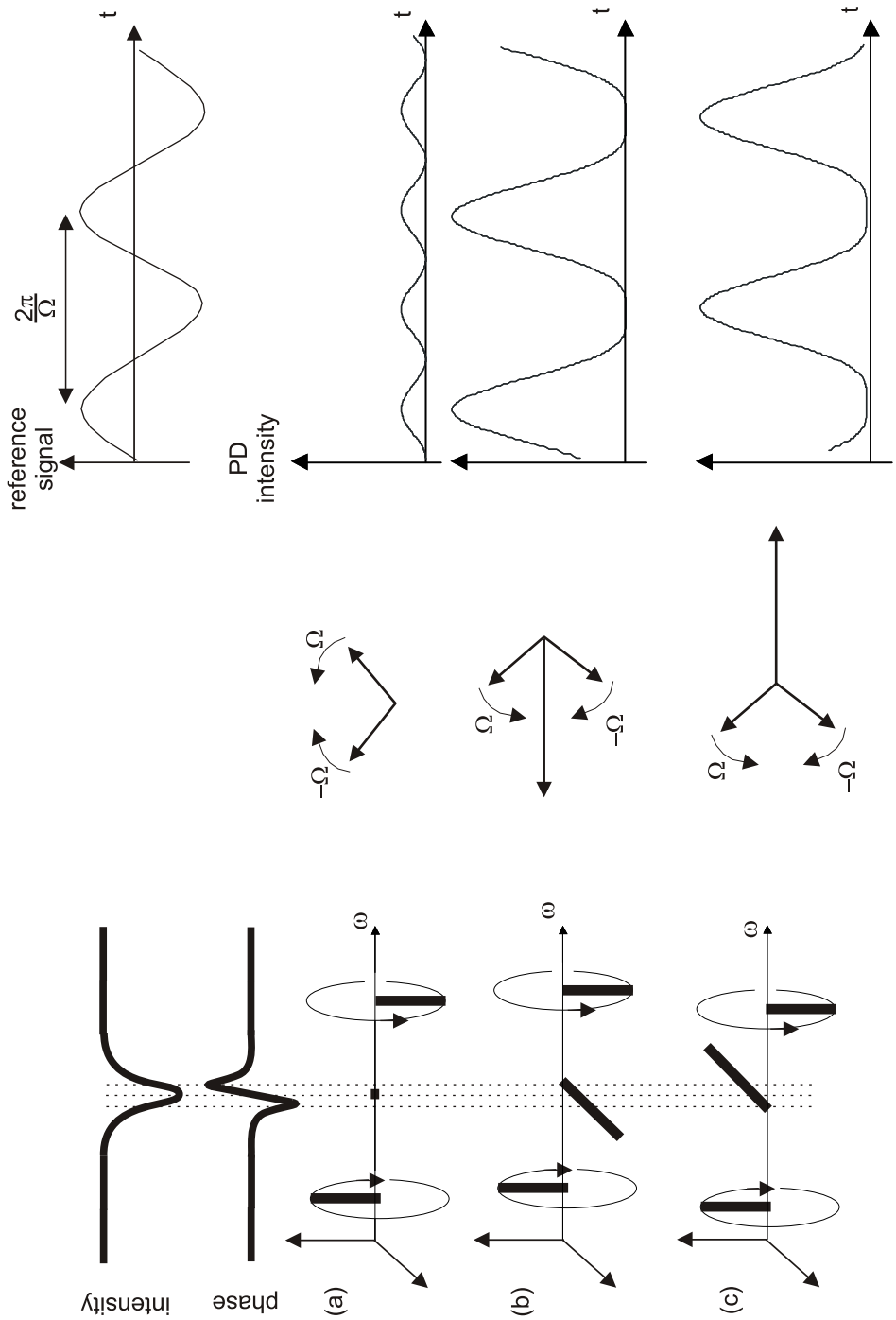

Figure 3.6: Left top: cavity reflection and phase shift. Right top: reference signal from the local oscillator. Left middle: reflected field amplitude when the cavity is held on resonance (a), below resonance (b) and above resonance (c). Middle: rotating field components, consequently. Right middle: square of the vector sum of these components the function of time.

Chapter 4

Active stabilization of the QED-cavity

In order to couple the cavity mode to a Cs-atom, the resonance frequency of the cavity must be stabilized to the atomic transition frequency. Additionally there should be the possibility to detune the cavity with respect to the atomic resonance by a few linewidths during the experiment.

The Pound-Drever-Hall method for laser-cavity stabilization, described in Chapter 3, can be applied to stabilize a cavity relative to a stable laser. An 852 nm laser can easily be absolutely stabilized using Cs saturation spectroscopy. But this laser cannot be used directly for locking the QED-cavity for the following reason. The PDH-lock implies that part of the laser beam enters the cavity. Due to the large resonant enhancement of the laser power inside the cavity the atomic transition would be saturated, even for the lowest possible incident power that could be used for locking.

To solve this problem we use an additional cavity lock-laser which is stabilized to a frequency far detuned from the Cs transition. The detuning of the lock-laser is chosen in such a way that the field inside the high finesse cavity produces an atomic scattering rate of the same order of magnitude as the scattering rate produced by the dipole trap. This requires the detuning to be of the order of tens of nanometer. An additional constraint is the wavelength dependence of the cavity finesse. This limits the useful detuning to about ± 20 nm. The absolute frequency stability of the 852 nm laser has to be transferred to the lock-laser.

4.1 Schematic of the stabilization setup

As a frequency standard we use a "probe-laser" locked to the Cs D_2 transition. To transfer this absolute frequency stability over the frequency gap of 16 nm to the lock-laser, which works at 836 nm, we have to use a *transfer cavity* [MAB99]. This transfer cavity is a low finesse cavity that is locked to the probe-laser at 852 nm, and the lock-laser, in turn, is stabilized onto this transfer cavity (see Fig.4.1). Therefore,

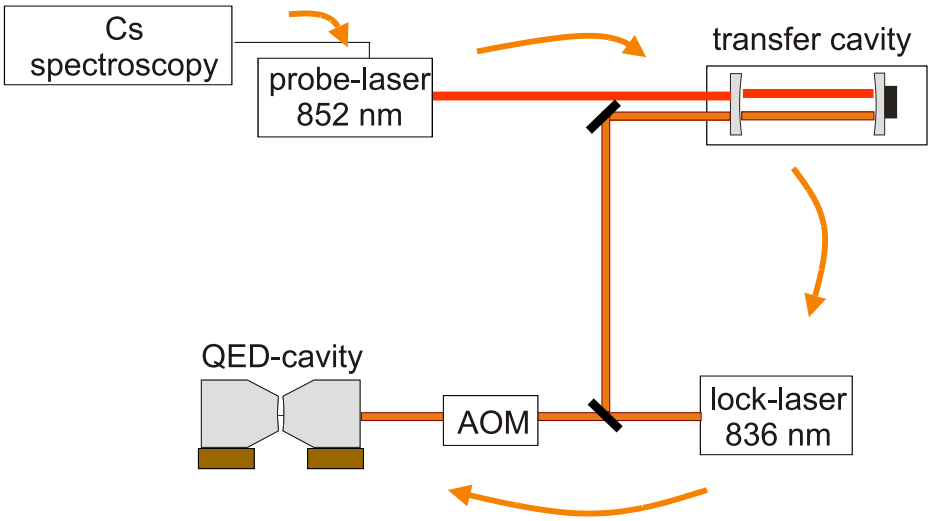

Figure 4.1: Schematic of the lock chain for stabilization of the QED-cavity. The probe-laser is locked to the Cs D_2 transition, the transfer cavity is locked to the probe-laser, the lock-laser is stabilized onto this transfer cavity, the QED-cavity is stabilized onto the lock-laser.

the absolute frequency stability of the Cs saturation spectroscopy is transferred to a wavelength where no atomic frequency standard is readily available.

The QED-cavity has to be resonant with the atomic transition. Since the FSR of the cavity strongly depends on the length of the cavity, it is not precisely known a priori. So one has to be able to stabilize the frequency of the lock-laser to any given frequency within one FSR of the QED-cavity (~ 0.5 GHz) at 836 nm.

Coarse adjustment is done by locking the lock-laser to different longitudinal modes of the transfer cavity. For fine adjustment we use an AOM. In order to reach any given frequency, the tuning range of the AOM has to cover at least one FSR of the transfer cavity. Since the tuning range of AOMs is typically limited to 200 MHz in double pass configuration, the FSR of the transfer cavity has to be of the order of 100 MHz.

4.2 Elements of the lock-chain

4.2.1 Transfer cavity

Design

As was mentioned in the previous section, the FSR of the transfer cavity has to be in the order of 100 MHz. This requires the cavity length to be roughly one meter. The stability criterion for symmetric resonators requires the radius of curvature of the cavity mirrors to be of the order of the magnitude of the length of the cavity. A standard laser mirror (99.8% reflectivity) and an outcoupler (98.5% reflectivity) with radii of curvature of 2 m are used for the transfer cavity (see Fig. 4.2). The exact length of the cavity was chosen to be 1.23 m in order to avoid degeneracy between the longitudinal and higher transversal modes.

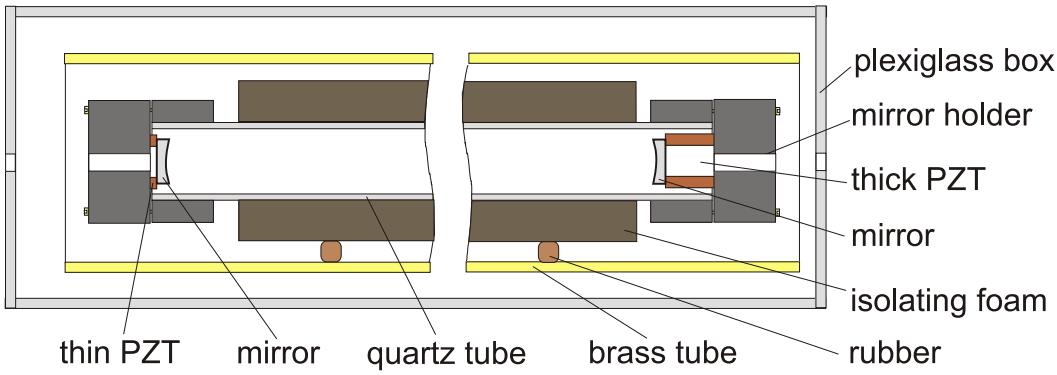

Figure 4.2: Design of the transfer cavity

To be able to scan the length of the cavity the mirrors are glued to PZTs. We use two types of PZTs, a thick one and a thin one. The PZTs themselves are glued to adjustable mirror holders.
A quartz glass tube was chosen to keep the distance between the mirrors, because quartz glass has a low thermal expansion coefficient ($\alpha = 0.45 \cdot 10^{-6}\ K^{-1}$). A tube of isolating foam, rubber knobs, a brass tube and a plexiglass box provide thermal, acoustic and vibration isolation of the cavity.

The measured linewidth of the cavity is (480 ± 10) kHz. This yields a finesse of the transfer cavity of 250.

Stabilization

The transfer cavity is locked to the stable probe-laser (see Fig. 4.3) using the Pound-Drever-Hall method.

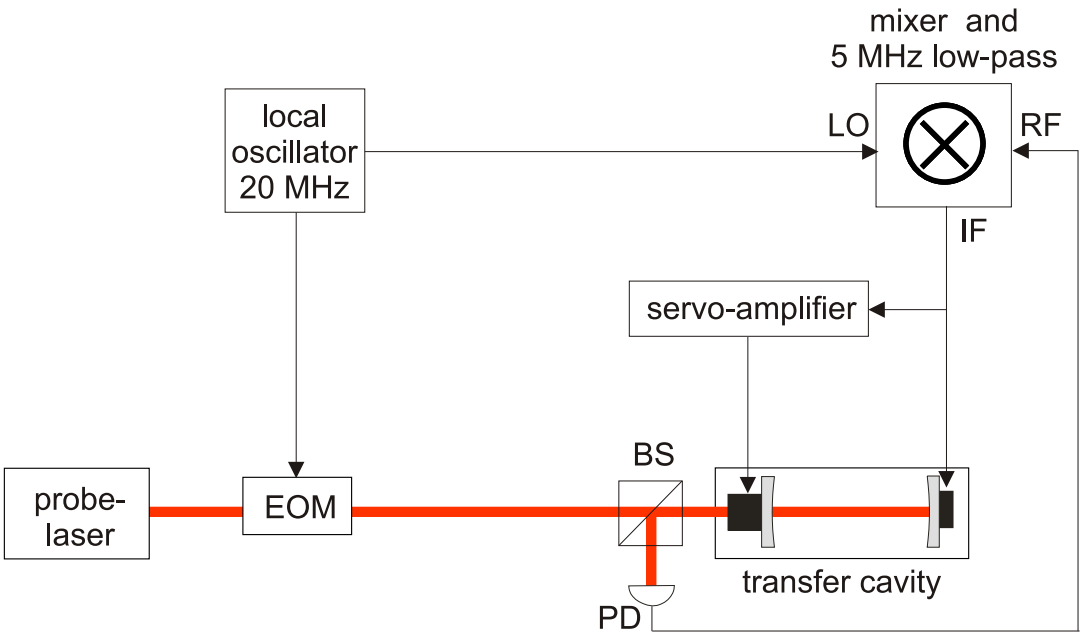

Figure 4.3: The transfer cavity is stabilized to the probe-laser using the PDH method

To create the necessary sidebands on the probe laser light we use an EOM which is driven by a 20 MHz signal from the local oscillator. The EOM phase modulates the probe laser beam which is coupled into the cavity. A fast photodiode measures the power of the reflected beam. The signal from this photodiode is mixed with the signal from the local oscillator to produce an error signal. Part of this error signal is sent though a proportional integral servo-amplifier to the thick PZT which compensates cavity length fluctuations in the frequency range of up to a few kHz. Another part of the error signal is sent directly to the thin-PZT to extend the servo bandwidth to several tens of kHz.

The necessary electronics for the PDH method is described in Appendix A.

Performance of the lock

The cavity was continuously locked to the probe-laser over a period of 3 hours until the probe-laser unlocked from the Cs-spectroscopy. The lock withstands loud acoustical noise and even slight knocks onto the optical table.

4.2.2 Lock-laser

Design

For the lock-laser we adopted the proven Littow-configuration (see Fig. 4.4) from the other diode lasers of the experiment. Here we used the SDL $5311 - G1$ laser diode operating at a wavelength of 836 nm. Single mode operation of the laser can be achieved by realizing frequency selective feedback. In Littrow-configuration the

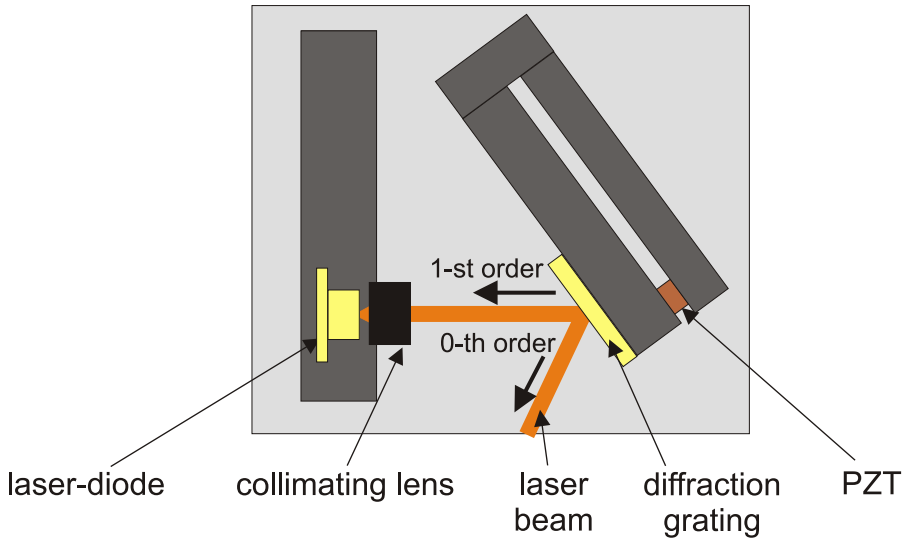

Figure 4.4: Diode laser in Littrow-configuration

light from the laser diode is collimated by a lens with a short focal length. The collimated beam is sent onto a grating in such a way that the first diffraction order is reflected back into the laser diode. The grating together with the back facet of the diode form an external resonator. The frequency selective feedback is done by adjusting the distance and the angle of the grating. The zeroth diffraction order is coupled out.
The frequency of the laser beam can be modulated by changing the voltage applied to the laser PZT (see Fig. 4.4) and directly modulating the current of the laser diode. The PZT has a modulation bandwidth of up to a few kHz. High frequency modulation, up to a few hundred MHz, are possible by changing the current of the laser diode.

Stabilization

The lock-laser is stabilized to the transfer cavity using the PDH method (see Fig. 4.5). To create the necessary sidebands on the lock-laser light we modulate

the current of the laser diode with 100 MHz. To implement the current modula-

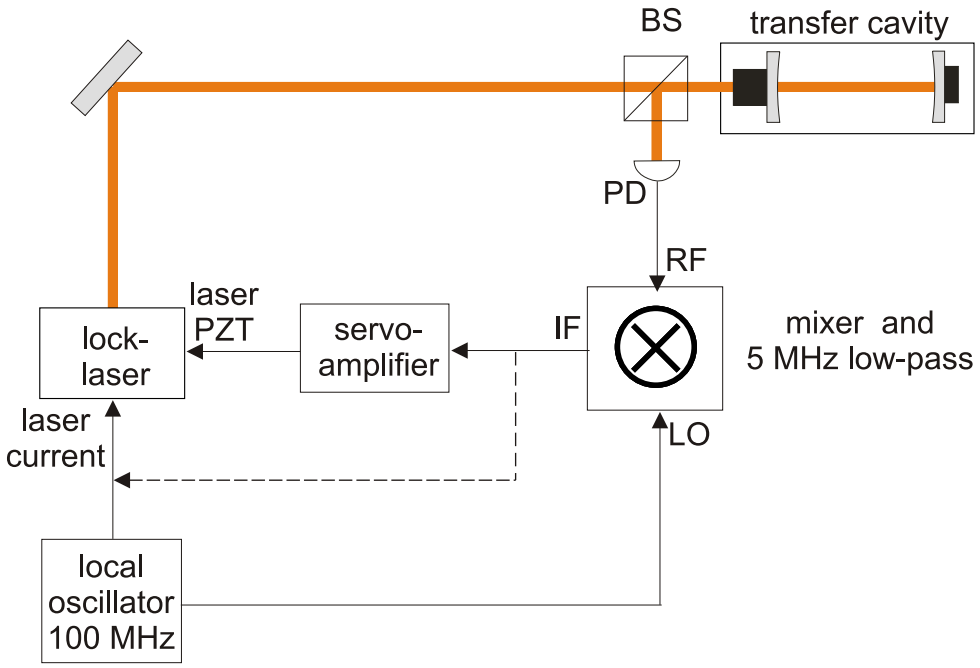

Figure 4.5: The lock-laser is stabilized to the transfer cavity using the PDH method

tion an additional current modulation port was added to the laser (see Fig. 4.6) ($L_1 = 1.8\ \mu$H, $L_2 = 12\ \mu$H and $C = 100\ \mu$F). A low-pass filter between the laser

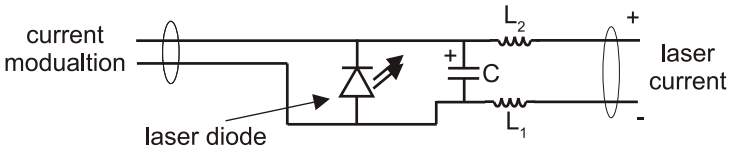

Figure 4.6: While the laser current port supplies the DC current for laser operation, the modulation port serves to modulate the laser at 100 MHz

current port and laser diode prevents the 100 MHz signal from entering the laser current controller.
The current modulation produces a phase-modulation of the laser beam. This beam is coupled into the transfer cavity. The reflected beam is detected by the same fast photodiode we use for the transfer cavity locking. The signals at 100 MHz from the lock-laser and at 20 MHz from the probe laser are far away from each other in frequency domain, so they can easily be separated by two filters. The 100 MHz signal from the fast photodiode is mixed with the local oscillator signal to produce an error signal. It is sent through the servo-amplifier onto the PZT of the laser

to compensate for the drifts of the laser frequency in the frequency region up to ~ 10 kHz. Later, part of the error signal will be picked off and sent into the current modulation port to extend the servo-bandwidth up to 1 MHz.

Performance of the lock

Up to now the lock-laser was stabilized using the PZT of the grating only. It locks, but it is very sensitive to acoustical and mechanical vibrations.

It is planned to use an additional servo-amplifier for the current feedback in order to increase the bandwidth of the lock up to a few MHz. The servo-loop has to be free of resonances within its bandwidth to work properly. A first prototype of the servo-amplifier for the current feedback was designed, built and tested with the probe laser. It has improved the performance of the lock.

4.2.3 QED-cavity

The lock chain described so far serves to stabilize the QED-cavity. A detailed description of the construction of the QED-cavity is given in Chapter 2.

Stabilization of the QED-cavity

The QED-cavity is locked to the lock-laser using the PDH-method (see Fig. 4.7).

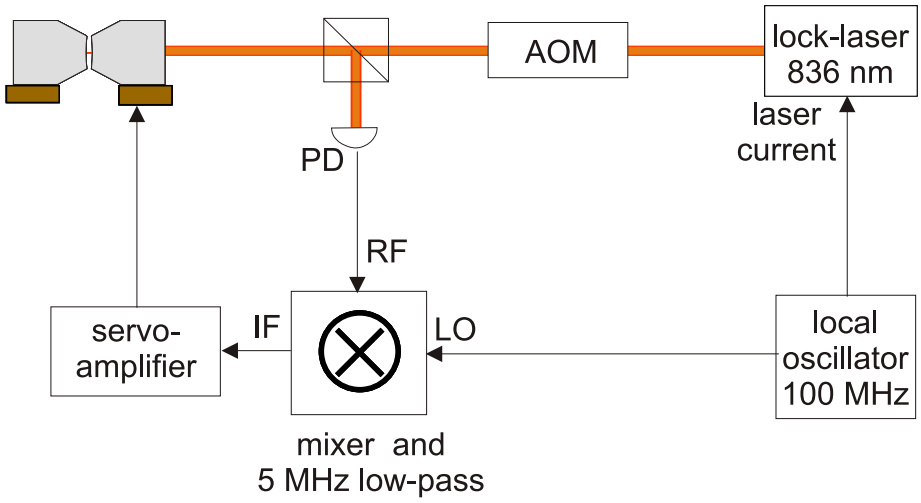

Figure 4.7: The QED-cavity is stabilized to the lock-laser using the PDH method

We use the phase modulated laser light from the lock-laser for the PDH stabilization of the QED-cavity. The phase modulated laser light is coupled to the cavity, and the

reflected beam is detected by a fast photo diode. The signal from the photodiode is mixed with the signal from the local oscillator, the same local oscillator that was used for stabilizing the lock-laser, to produce an error signal. The resulting error signal is sent through a servo-amplifier onto the cavity PZTs to lock the cavity.

Performance of the lock

A specially designed abberations compensated telescope (see Fig. 2.9) allowed us to couple about 95% of the laser power into the TEM_{00} mode of the resonator. This made it possible to produce an error signal from the QED-cavity (see Fig. 4.8). The

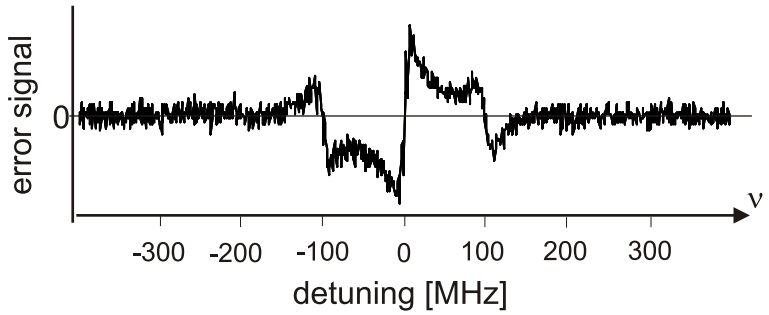

Figure 4.8: Error signal used to lock the QED-cavity

central part of the error signal has a dispersive shape, necessary for locking. The signal to noise ratio was quite low. Fig. 4.8 represents 8-times averaged error signal. Nevertheless, the cavity was continuously locked for about a quarter of an hour, until it was manually unlocked. The lock withstands loud acoustical noise and even slight knocks onto the optical table.

Now the lock has to be optimized by reducing the power of the lock laser and increasing the signal to noise ratio. The power of 10 μW, which was used for the first tests, will produce a scattering rate inside the QED-cavity of about 200 times the scattering rate in the dipole trap. In order to have a scattering rate of the same order of magnitude as in the dipole trap, the lock-laser power has to reduced down to about 500 nW. The signal to noise ratio will be increased by replacing the fast photodiode by an avalanche photo diode (APD). An APD itself is more sensitive than a photo diode due to the internal amplification. Additionally, the amplification will be resonant with the 100 MHz modulation frequency of the lock-laser. This resonant enhancement will additionally increase the signal to noise ratio.

4.3 Lock-chain

An overview of the entire lock-chain is given in Fig. 4.9. Up to now all the locks of the chain were tested and optimized separately. The next step will be to optimize the performance of the lock-chain as a whole.

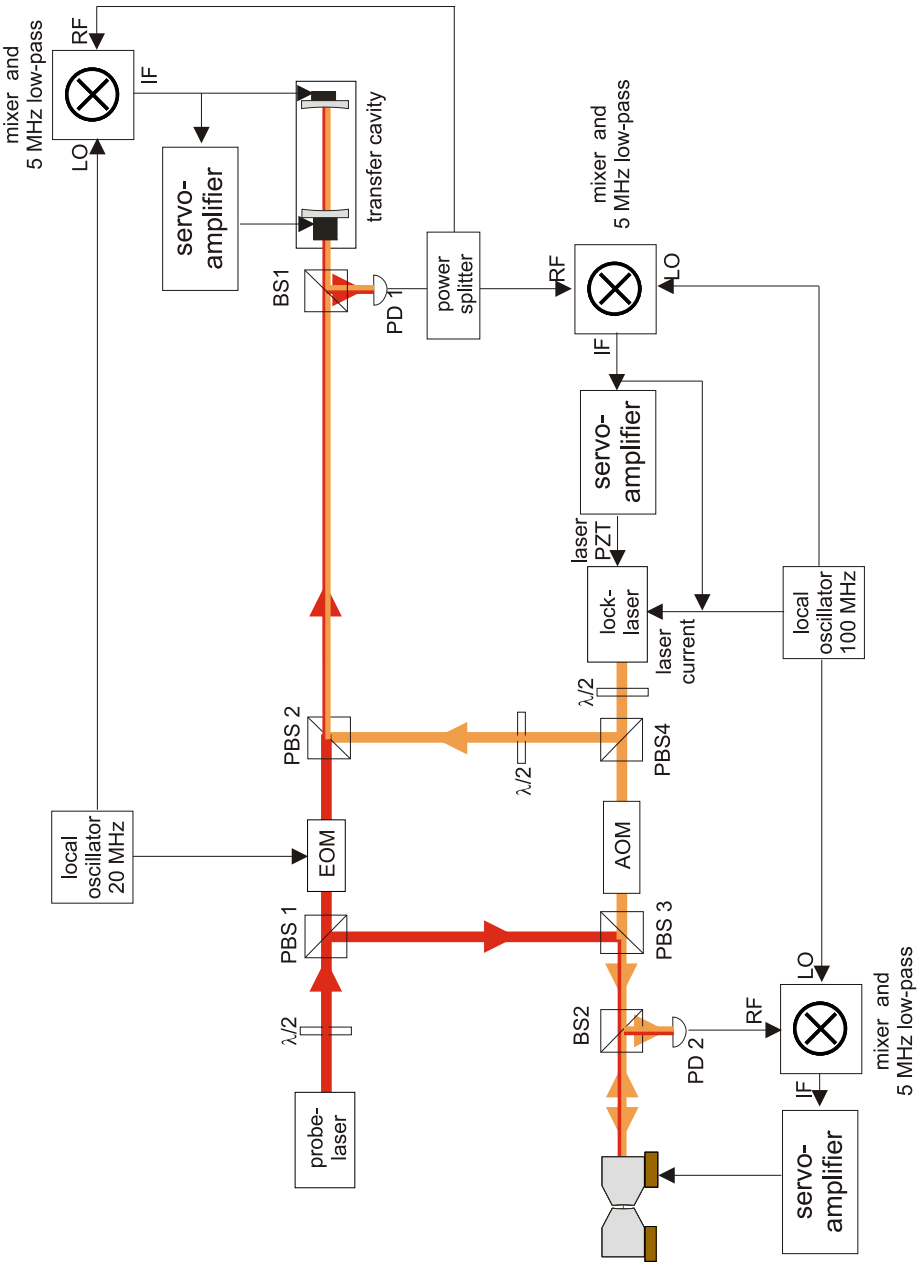

Figure 4.9: Detailed overview of the lock-chain for stabilization of the QED-cavity

Summary and outlook

The goal of this work was the construction and stabilization of a high-finesse microresonator for the use in cavity QED experiments with single neutral atoms. There, one of the most demanding experimental tasks is to reach the "strong coupling regime", where the coupling strength between atoms and cavity exceeds both resonator losses and the atomic spontaneous decay rate. The strategy to achieve this goal is to increase the finesse of the cavity, which makes for a small cavity decay rate, and to reduce the mode volume in order to increase the coupling strength.

A working prototype of a suitable cavity with a finesse of 94.000 and a length of 250 μm has been built and characterized. These parameters already allow us to achieve the regime of strong coupling ($g_0/2\pi = 11$ MHz, $\kappa/2\pi = 3$ MHz, $\gamma/2\pi = 5$ MHz).
A specially designed telescope allowed us to couple about 95% of the laser power into the TEM_{00} mode of the resonator. This made it possible to produce an error signal and to lock the cavity.

The cavity has to be continuously stabilized to the atomic resonance. For this purpose a far detuned lock-laser has to be used, to avoid any interaction with the atoms inside the cavity. But there are no readily available possibilities to realize a spectroscopical stabilization of this far detuned laser. That is why a chain of Pound-Drever-Hall locks has been set up to transfer the stability from a resonant laser to the far detuned lock-laser via an additional low finesse transfer cavity.

The major part of my work was devoted to the realization of this lock-chain. I have set up the 836 nm lock-laser (a diode laser in Littrow configuration), a suitable transfer cavity, and all the necessary optics and electronics for the PDH locks. All these PDH locks have been separately tested and optimized.

The next steps will be to complete the whole lock chain. Additionally, we are currently optimizing the cleaning methods of the high reflecting mirrors of the microcavity. This could allow us to achieve an even higher finesse.

The cavity was designed to be compatible with the current setup for single atoms (see Fig. 4.10), and its design allows us to place it close to the magneto optical

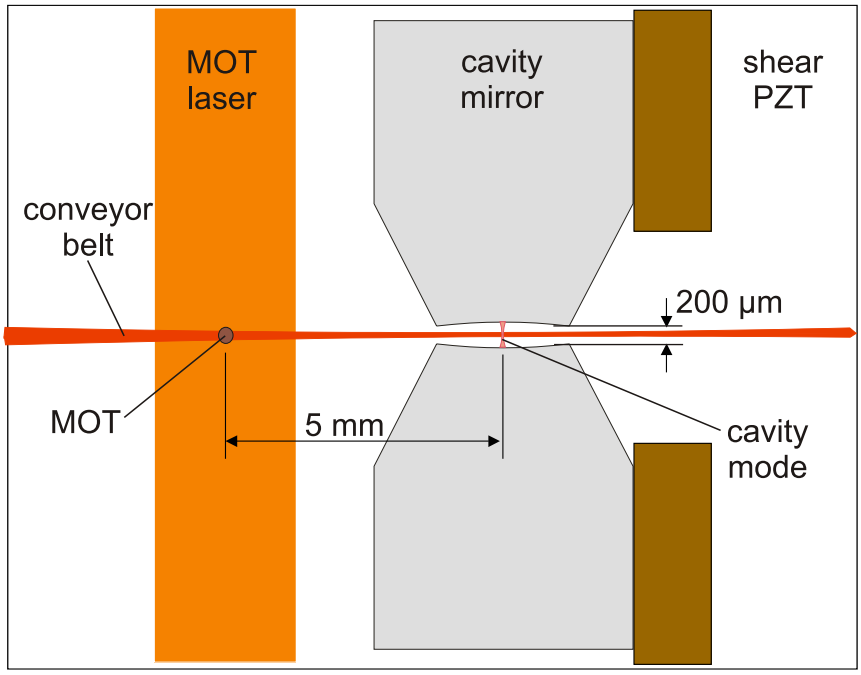

Figure 4.10: Schematic of the planned experiment. The optical conveyor belt will transport atoms from the MOT into the cavity mode.

trap. The optical conveyor belt will transport atoms from the MOT into the cavity mode. This scheme promises to realize full control of the *atom-cavity* interaction. The possibility to deterministically deliver exactly two atoms to a desired position inside the high finesse cavity promises to realize a controlled *atom-atom* interaction via "sharing" the same optical photon by both atoms. This is a necessary step for the implementation of a two-qubit quantum gate, in which neutral atoms are carriers of quantum information.

Appendix A

Pound-Drever-Hall electronics

A.1 Local oscillator

The heart of the local oscillator (LO) circuit is a voltage controlled oscillator (VCO). This device produces a sine signal, whose frequency is controlled by a voltage applied to the control port. A block diagram of the LO circuit is presented in Fig. A.1.

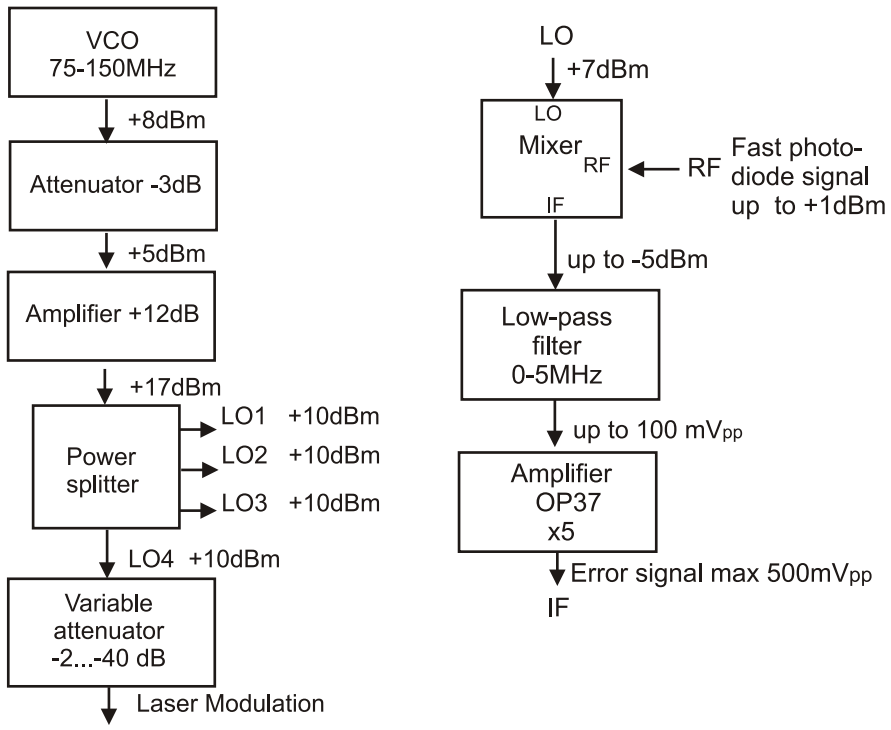

Figure A.1: Block diagram of the local oscillator circuit and of the mixer circuit, respectively

The signal from the VCO is amplified and then divided by a power splitter into four output ports, one for laser modulation and three as reference signals for mixers. The signals for mixers have fixed amplitudes. A variable attenuator allows to change the amplitude of the laser modulation.
Two LO-circuits were built (see Fig. A.3 for a schematic) - one for $75 - 150$ MHz and another one for $15 - 25$ MHz.

A.2 Mixer

The mixer (see Fig. A.1 for a block diagram) has two input ports: the signal from the fast photodiode (RF) and for the reference local oscillator (LO). The mixer produces signals at sum and difference frequencies. This signal is sent through a low-pass filter to filter out the frequencies above 5 MHz. The low frequency signal is amplified and sent into the output port of the mixer box (IF). See Fig. A.4 for the schematic.

Tests showed that the mixer has a bandwidth of $0 - 5$ MHz, which is more than sufficient for locking.

A.3 Resonantly driven EOM

An EOM is used to phase-modulate the probe-laser beam. The modulation index is proportional to the amplitude of the RF-signal applied to the EOM.
The RF-generator is designed to work with a 50 Ω load. Electrically an EOM looks like a capacitor. One cannot directly connect the EOM to the output of the generator because the EOM produces only a reactive load. To achieve impedance matching between the EOM and the generator, the EOM is inductively coupled to the RF-generator (see Fig. A.2). The EOM LC-circuit is adjusted to be resonant with the modulation frequency. Due to the resonant enhancement of the voltage in

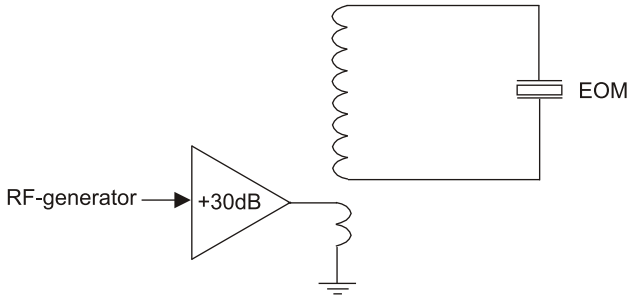

Figure A.2: Resonantly driven EOM

this circuit, one can work with moderate power of the RF-generator (2 W) and have a reasonable modulation index.

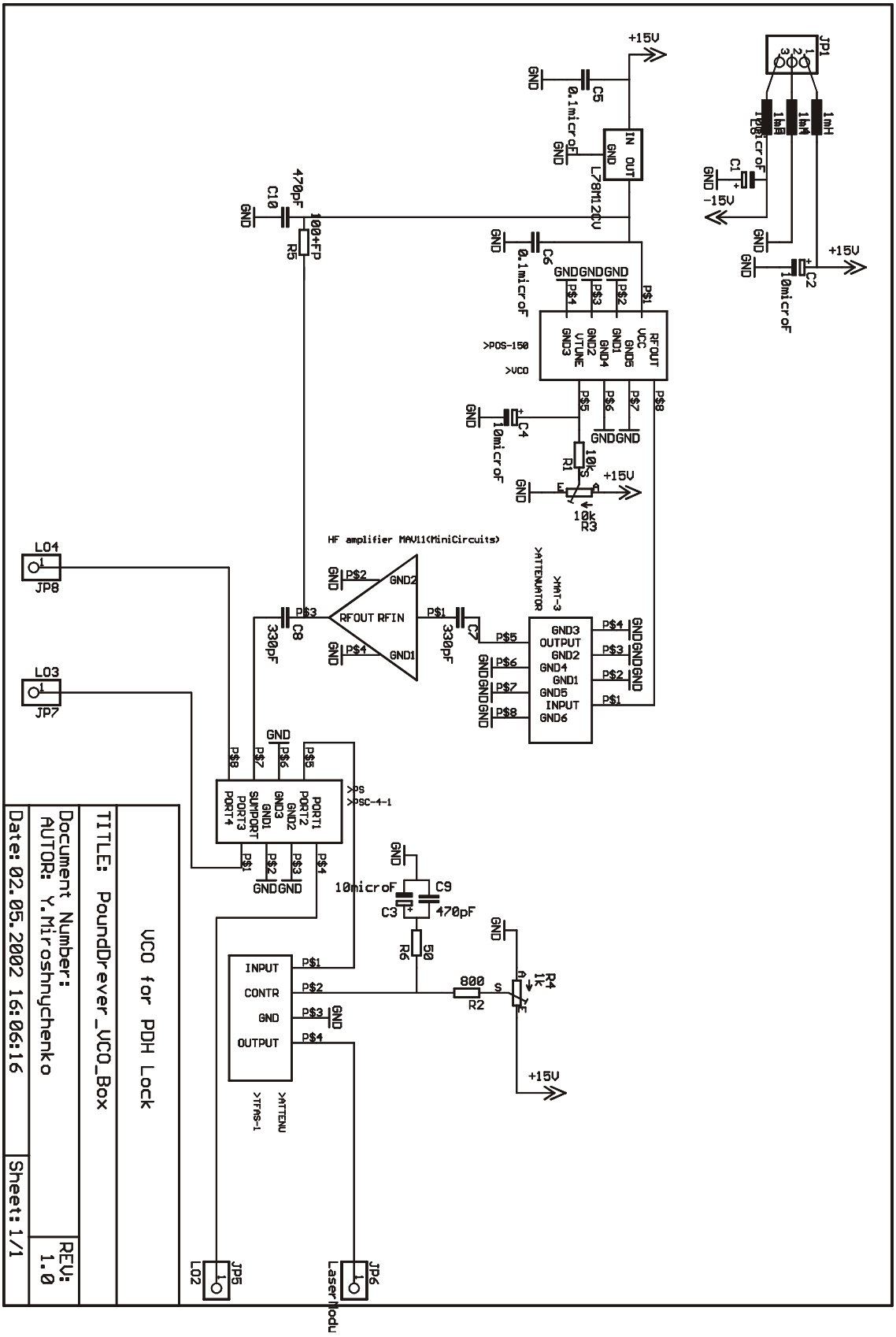

Figure A.3: Schematic of the local oscillator circuit. $R4$ allows to adjust the amplitude of the laser modulation. R_3 allows to adjust the frequency of the VCO.

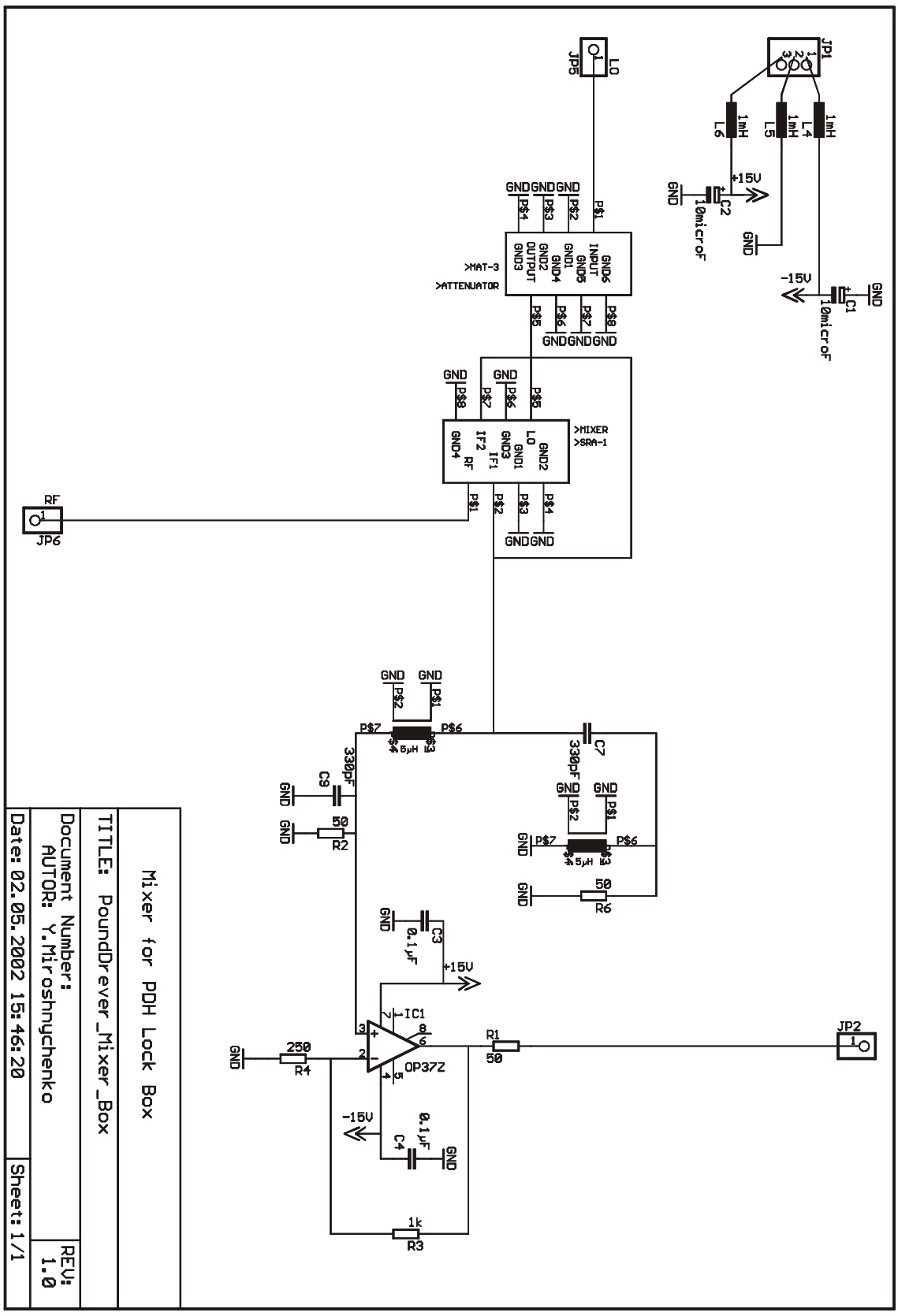

Figure A.4: Schematic of the mixer circuit

Bibliography

[Bla00] R. Blatt, *Push-button entanglement*, Nature **404**, p. 231 (2000)

[Bre99] G. Brennen, C. Caves, P. Jessen and I. Deutsch, *Quantum Logic Gates in Optical Lattices*, Phys. Rev. Lett. **82**, p. 1060 (1999)

[Dre83] R. Drewer and J. Hall, *Laser phase and frequency stabilization using an optical resonator*, Appl. Phys. B **31**, p. 97 (1983)

[Fre00] D. Frese, B. Ueberholz, S. Kuhr, W. Alt, D. Schrader, V. Gomer and D. Meschede, *Single Atoms in an Optical Dipole Trap: Towards a Deterministic Source of Cold Atoms*, Phys. Rev. Lett. **85**(18), p. 3777–3780 (2000)

[Gri95] J. Gripp, S. Mielke and L. Orozco, *Cascaded optical cavities with two-level atoms: Steady state*, Phys.Rev. **51**, p. 4974 (1995)

[Hag97] E. Hagley, X. Maitre, G. Nogues, C. Wunderlich, M. Brune, J. Raimond and S. Haroche, *Generation of Einstein-Podolsky-Rosen Pairs of Atoms*, Phys. Rev. Lett. **79**(1), p. 1–5 (1997)

[Hoo00] C. Hood, T. Lynn, A. Doherty, A. Parkins and H. Kimble, *The Atom-Cavity Microscope: Single Atoms Bound in Orbit by Single Photons*, Science **287**, p. 1447–1453 (2000)

[Hor02] P. Horak, H. Ritsch, T. Fischer, P. Maunz, T. Puppe, P. Pinkse and G. Rempe, *An optical kaleidoscope using a single atom*, Phys. Rev. Lett. **88**, p. 043601 (2002)

[Jak99] D. Jaksch, H.-J. Briegel, J. Cirac, C. Gardiner and P. Zoller, *Entanglement of atoms via cold controlled collisions*, Phys. Rev. Lett. **1975**, p. 1975 (1999)

[Jay63] E. Jaynes and F. Cummings, Proc.IEEE **51**, p. 89 (1963)

[Kuh01] S. Kuhr, D. Schrader, W. Alt, M. Mueller, V. Gomer and D. Meschede, *Deterministic delivery of a single atom*, Science **293**, p. 278 (2001)

[Mab99] H. Mabuchi, J. Ye and H. Kimble, *Full observation of single-atom dynamics in cavity QED*, Applied Physics B (Lasers and Optics) **B68**(6), p. 1095–108 (1999)

[Mon02] C. Monroe, *Quantum information processing with atoms and photons*, Nature **416**, p. 238 (2002)

[Pel95] T. Pellizari, S. A. Gardiner, J. I. Cirac and P. Zoller, *Decoherence, Continous Observation and Quantum Computing: A Cavity QED Model*, Phys. Rev. Lett **75**, p. 3788 (1995)

[Pin00] P. Pinske, T. Fischer, P. Maunz and G. Rempe, *Trapping an atom with single photons*, Nature **404**, p. 365 (2000)

[Rai01] J. Raimond, M. Brune and S. Haroche, *Manipulating quantum entanglement with atoms and photons in a cavity*, Rev. Mod. Phys. **73**, p. 565 (2001)

[Rau00] A. Rauschenbeutel, G. Nogues, S. Osnaghi, P. Bertet, M. Brune and S. Haroche, *Step-by-Step engineered multiparticle entanglement*, Science **288**, p. 2024 (2000)

[Sac00] C. A. Sackett, D. Kielpinski, B. E. King, C. Langer, V. Meyer, C. J. Myatt, M. Rowe, Q. A. Turchette, W. M. Itano, D. Wineland and C. Monroe, *Experimental entanglement of four particless*, Nature **404**, p. 256 (2000)

[Sch01] D. Schrader, S. Kuhr, W. Alt, M. Mueller, V. Gomer and D. Meschede, *An optical conveyor belt for single neutral atoms*, Appl. Phys. B **73(8)**, p. 819 (2001)

[Sie86] A. Siegman, *Lasers*, University Science Books, Sausalito, California (1986)

[You00] L. You and M. Chapman, *Quantum entanglement using trapped atomic spins*, Phys. Rev. **A62**, p. 052302 (2000)

Acknowledgment

There are many people who have helped to make this thesis possible. First of all, I would like to thank Prof. Meschede who opened for me the possibility to work in this absolutely fascinating and exciting area of quantum optics and quantum information. My thanks to prof. Buse, for taking the role of a co-referent for my thesis.

I would like to thank our Ph.D. students who have opened for me lots of secrets of a laboratory life: Stefan Kuhr with his endless optimism, especially, during the night, when we have observed the the first transmission spectrum of the supercavity; Wolfgang Alt with his patience during teaching me that electronics is not a nightmare, especially, during debugging the servo loop of the lock-laser; and Dominik Schrader who was teaching me "not being afraid to ask questions", which helped me a lot afterwards.

My great thanks to Dr. Viktor Gomer who made it possible for me to stresslessly start my experimentalist life during my Ferienpraktikum two years ago and for his readiness for discussions all the time. My thanks to Dr. Arno Rauschenbeutel for his fruitful discussions and comments.

I would like to acknowledge Daniel Frese who, actually, started the whole story three years ago with his phrase: "There is a guy, Stefan Kuhr, in the lab who builds a quantum computer." I was young and naive, but one day the dreams come true...

My thanks to our Diploma students Igor Dotsenko and Wenjamin Rosenfeld for interesting discussions, especially, during my writing of the Diploma thesis.

I would like to thank all the members of the group and the institute staff, who was not jet mentioned here, for keeping this pleasant atmosphere in the institute.

My great thanks once more to all the guys who have critically read the drafts of this work: Stefan Kuhr, Wolfgang Alt, Dominik Schrader, Viktor Gomer and Igor Dotsenko.

Without the love and support of my parents, who have always encouraged my enthusiasm, I would not have made it this far.

My thanks to Aska Dolinska from the Australian National University for the inspiration during this work and for "not loosing the faith".